

Recyclable vitrimer-based printed circuit boards for sustainable electronics

Received: 1 September 2023

Accepted: 26 March 2024

Published online: 26 April 2024

 Check for updates

Zhihan Zhang  ¹, Agni K. Biswal  ², Ankush Nandi  ², Kali Frost³, Jake A. Smith  ^{1,3}, Bichlien H. Nguyen  ^{1,3}, Shwetak Patel^{1,4}, Aniruddh Vashisth  & Vikram Iyer  ¹

Printed circuit boards (PCBs) are ubiquitous in electronics and make up a substantial fraction of environmentally hazardous electronic waste when devices reach end-of-life. Their recycling is challenging due to their use of irreversibly cured thermoset epoxies in manufacturing. Here, to tackle this challenge, we present a PCB formulation using transesterification vitrimers (vPCBs) and an end-to-end fabrication process compatible with standard manufacturing ecosystems. Our cradle-to-cradle life-cycle assessment shows substantial environmental impact reduction of the vPCBs over conventional PCBs in 11 categories. We successfully manufactured functional prototypes of Internet of Things devices transmitting 2.4 GHz radio signals on vPCBs with electrical and mechanical properties meeting industry standards. Fractures and holes in vPCBs are repairable while retaining comparable performance over multiple repair cycles. We further demonstrate a non-destructive recycling process based on polymer swelling with small-molecule solvents. Unlike traditional solvolysis recycling, this swelling process does not degrade the materials. Through dynamic mechanical analysis, we find negligible catalyst loss, minimal changes in storage modulus and equivalent polymer backbone composition across multiple recycling cycles. This recycling process achieves 98% polymer recovery, 100% fibre recovery and 91% solvent recovery to create new vPCBs without performance degradation. Overall, this work paves the way for sustainability transitions in the electronics industry.

Electronics have become an integral part of modern life in everything from smartphones and laptops to state-of-the-art industrial, scientific and medical technologies. However, when electronics reach their end of life due to obsolescence or damage, they become electronic waste (e-waste) and pose substantial environmental hazards. E-waste contains a complex toxic mixture of metals, silicon integrated circuits (ICs), glass fibres, thermoset polymers, flame retardants and more. This waste can pollute the air, soil and water, posing significant hazards for surrounding communities^{1–3}. With over 53.6 million metric tons (Mt)

generated in 2019 alone⁴, e-waste is among the fastest-growing waste streams globally⁵ and a matter of global concern⁶.

In response, efforts are underway to reduce e-waste by transitioning to a circular economy where electronics can be transformed into secondary raw materials. A key challenge in achieving circular manufacturing is the recycling of printed circuit boards (PCBs). PCBs are ubiquitous in electronics and rank within the world's top 100 most traded products⁷. They form the physical substrate upon which chips are mounted and connected with metal traces patterned on their

¹Paul G. Allen School of Computer Science and Engineering, University of Washington, Seattle, WA, USA. ²Department of Mechanical Engineering, University of Washington, Seattle, WA, USA. ³Microsoft Research, Redmond, WA, USA. ⁴Department of Electrical and Computer Engineering, University of Washington, Seattle, WA, USA.  e-mail: vashisth@uw.edu; vsiyer@uw.edu

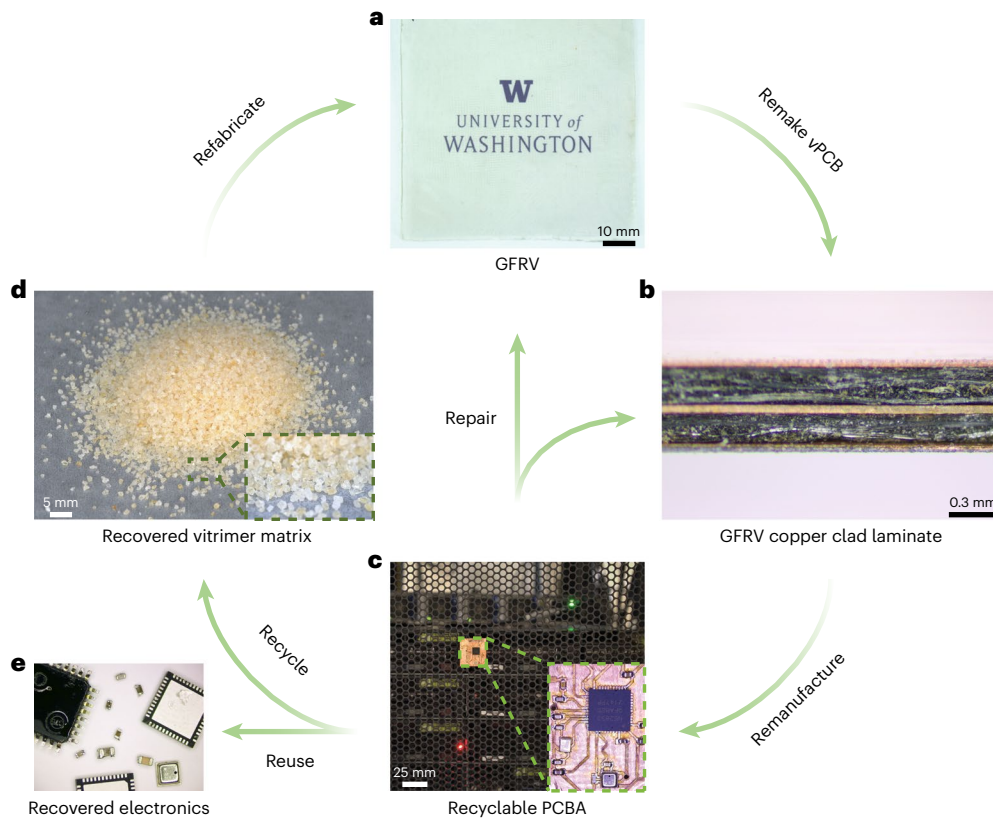


Fig. 1 | Transesterification vitrimer-based fully recyclable PCB. Conceptual diagram showing the closed-loop repair and recycling of vPCB. **a**, GFRV composite. **b**, Cross-sectional view of a three-layer vPCB. **c**, Photograph of a vPCB-based recyclable IoT sensor next to a server. The printed circuit board assembly (PCBA) can be repaired if warping or damage occurs in the base

material. After the device is decommissioned, the substrate materials can be recycled and the electronic components can be reused. **d**, Recovered vitrimer from obsolete vPCBs after drying and pulverizing, which can be reused to fabricate new GFRVs. **e**, Recovered electronics components from obsolete vPCBs that can be reused directly in new devices.

surface. PCBs are most commonly composite materials made of glass fibre weaves within a flame-retardant thermoset epoxy matrix (FR-4). Previous recycling efforts have focused on the recovery of intact ICs and high-value minerals such as gold and copper^{8,9}; however, 70% of a PCB's volume and mass are made up of dielectric substrates¹⁰.

Achieving scalable and circular PCB manufacturing is challenging. The irreversibly cured thermosets in conventional PCBs that give them fire and chemical resistance required for compatibility with the existing electronic manufacturing services (EMS) ecosystem make them incredibly challenging to recycle. An effective recycling process should be repeatable and non-destructive to produce high-quality raw materials. This prevents the use of thermoplastics which are damaged during reprocessing¹¹. Previous recycling attempts such as mechanical grinding, thermal decomposition (pyrolysis) or chemical dissolution in strong solvents (solvolytic) cause substantial material damage^{12,13}, require high energy costs¹⁴, or solvents that are not reusable or produce hazardous by-products^{14–17}. Previous work has explored alternative water-soluble^{18–23} and healable materials²⁴; however, these sacrifice compatibility with chemical etching, electroplating and elevated temperatures for soldering in EMS processes, which limits their potential to scale. In addition, these materials do not meet the electrical and mechanical standards for moisture absorption, flammability, dielectric constant, loss tangent and other criteria needed to produce high-speed circuits common in modern electronics.

In this Article, we introduce a sustainable PCB solution using transesterification vitrimers (vPCBs). Associative exchange reactions in dynamic covalent adaptive networks (CANs) enable reversible crosslinking at elevated temperatures²⁵. Vitrimers fall under this

category of CANs and engage in dynamic covalent bond exchange when heated, facilitating repair and reuse with minimal property loss^{26,27}.

Figure 1 illustrates our fully circular manufacturing and recycling pipeline which highlights our key contributions. First, we create glass fibre-reinforced vitrimer (GFRV) composites and develop an end-to-end vPCB fabrication process compatible with current EMS ecosystems including multilayer copper lamination, chemical etching, laser structuring, electroless plating and soldering. We characterize our vPCBs demonstrating that they meet industry standards and demonstrate a fully functional Internet of Things (IoT) sensor capable of transmitting 2.4 GHz wireless signals. Second, we leverage the bond exchange capabilities of vitrimers to repair physically damaged vPCBs while maintaining their mechanical and electrical properties over more than four repair cycles.

Third, we develop an end-to-end recycling process for our vPCBs. We observe that certain small-molecule solvents cause the vitrimer to swell. We leverage this swelling to deconstruct transesterification vitrimer composites with solid inclusions and metal attachments. We confirm that recycling causes negligible catalyst loss, minimal change in crosslink density and no changes in molecular structure. We further verify that recycled vPCBs have mechanical and electrical properties on par with the originals. Our recycling process achieves 98% recovery of the vitrimer polymer and 100% recovery of glass fibres, and even a 91% recovery of the solvent which we successfully reuse. We perform a comprehensive cradle-to-cradle life-cycle assessment (LCA) leveraging industrial-scale models to compare the environmental impact of our vPCB remanufacturing and recycling systems with conventional PCBs. Our results show 47.9% improvement in global warming potential (GWP), 65.5% in ozone depletion potential and 80.9% in human cancer

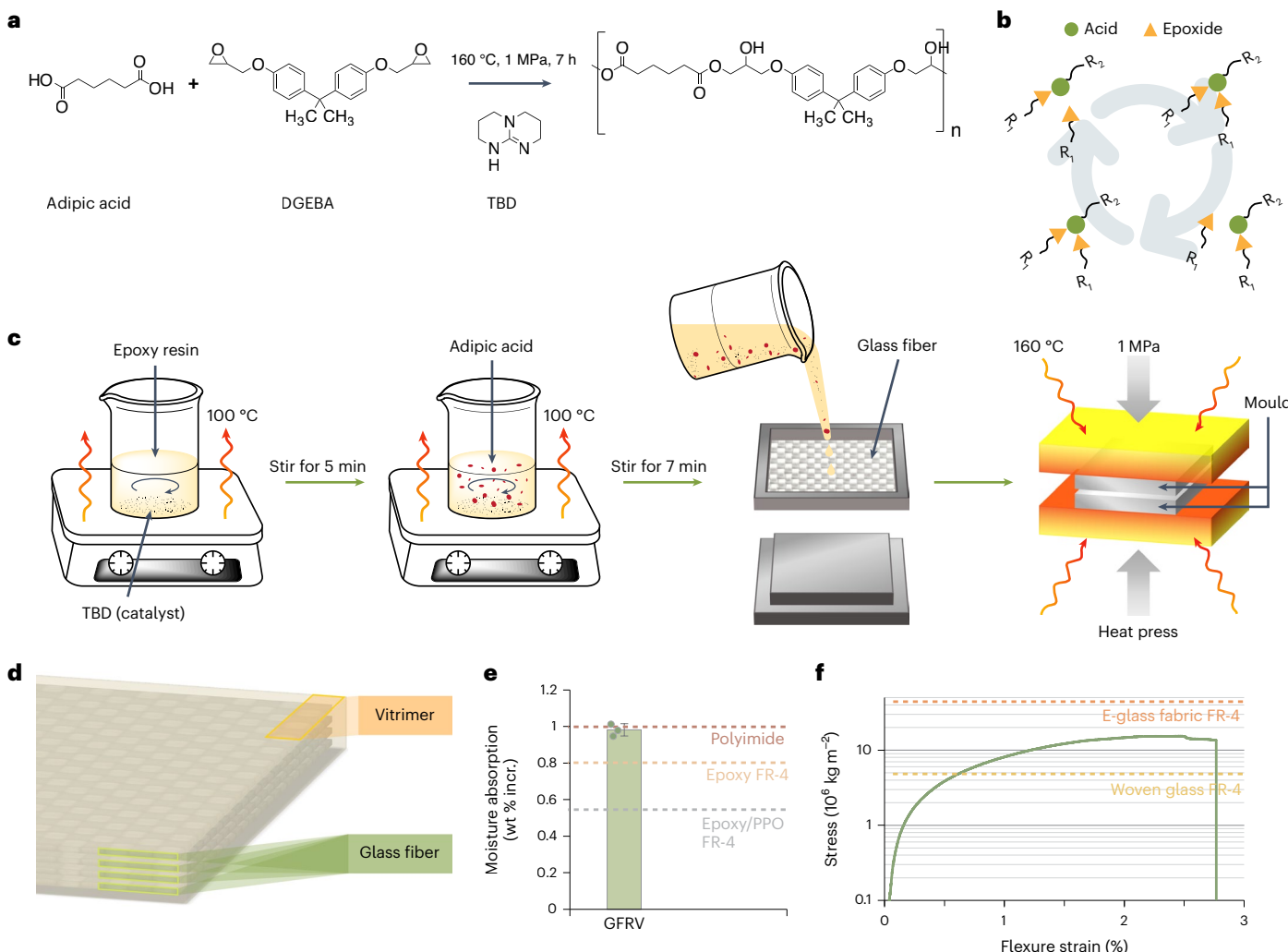


Fig. 2 | Glass fibre-reinforced vitrimer composite. **a**, Reaction of transesterification vitrimer under heat and pressure. **b**, Bond exchange via transesterification in vitrimer networks enables healing and recyclability when heated. Properties can be tuned by changing the functional chains R_1 and R_2 in the epoxide and acid used. **c**, Schematic of the fabrication process of GFRV.

d, Schematic of four-layer glass fibre GFRV. **e**, Characterized moisture absorption of GFRV compared to the PCB standards; data are mean \pm s.d. of 3 GFRV specimens ($N = 3$). **f**, Characterized flexural strength of GFRV compared to the PCB standards of woven glass FR-4 and woven e-glass fabric FR-4.

toxicity emissions for our recycling process compared with conventional PCB end-of-life disposal.

Results

Glass fibre-reinforced vitrimer composites

To enable circularity, we seek to disassemble the entire board into its constituent raw materials without damage for reuse. While the electronics and copper traces can be recovered using thermal exposure²⁸ or chemical etchants²⁹, the dielectric substrate material remains. The most common material, FR-4, consists of a glass fibre weave impregnated with a thermoset epoxy resin. The covalent crosslinks of these thermosets give the material high structural integrity, chemical stability and resistance to temperature. These properties, however, present a trade-off for recycling: the material's robustness makes it difficult to separate the epoxy and glass fibres for reuse.

Inspired by recent advancements in healable materials, we take a different approach and re-engineer PCBs using polymers with dynamic CANs; vitrimers are a special class of CANs with a thermosetting macromolecular network with healing abilities. This property also enables entirely new capabilities such as remanufacturing, in which holes can be refilled and segments can be tiled together without transforming them into raw materials. The ability to reuse vitrimers as secondary

raw materials also opens the possibility for effective recycling if they can be non-destructively separated from the glass fibres. We focus on vitrimers with associative exchange reactions over dissociative mechanisms due to their ability to maintain a consistent crosslink density over multiple recycling cycles.

Our vitrimer polymers are synthesized from a bifunctional epoxide (DGEBA) and an acid (adipic acid) in the presence of a catalyst triazabicyclodecene (TBD). The chemical structures for the reaction are shown in Fig. 2a. In contrast to previous attempts at integrating healable polymers into circuits³⁰, our vitrimer chemistry is optimized for similarity to conventional FR-4 by choosing a bisphenol-A epoxide which is typically used in PCBs³¹. The normalized stress-relaxations at temperatures ranging from 140 °C to 240 °C and the characterized storage modulus and tan delta for vitrimers with a 5 mol % catalyst concentration are shown in Extended Data Fig. 1. It is noteworthy that by tuning the specific components and functional groups (Fig. 2b), a wide variety of different properties can be achieved^{32–34}, such as a higher glass transition temperature (T_g) of 146 °C³⁵.

Our recyclable GFRV composites are created using a scalable fabrication process similar to conventional FR-4 fabrication shown in Fig. 2c (see Methods for details). Figure 2d schematically illustrates the structure of the resulting GFRV.

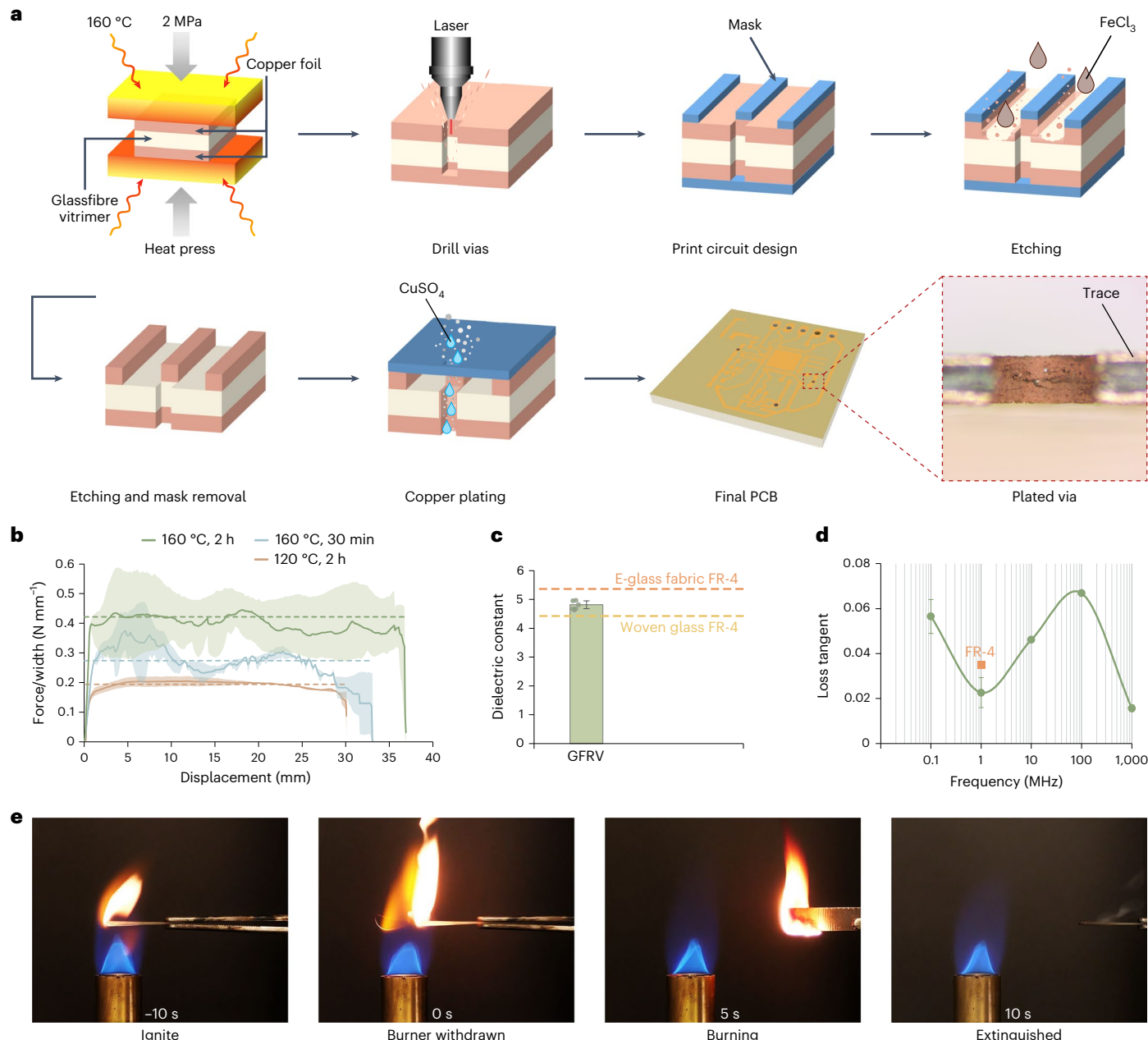


Fig. 3 | Characterization of vPCB. **a**, Schematic of the scalable manufacturing process of vPCB. **b**, Curves of the peeling force per width of copper-clad laminates versus displacement at various heat-press temperatures and times ($N = 3$ specimens per condition, shaded region indicates maximum and minimum values per condition). **c,d**, Characterized dielectric constant (**c**) and loss tangent (**d**) of vPCB compared to the PCB standards of various FR-4 types; data are mean \pm s.d. of $N = 6$ (**c**) and $N = 3$ (**d**) vPCB specimens. **e**, Flammability test of vPCB. The sample is retracted after 0 s to move it away from the burner.

values per condition). **c,d**, Characterized dielectric constant (**c**) and loss tangent (**d**) of vPCB compared to the PCB standards of various FR-4 types; data are mean \pm s.d. of $N = 6$ (**c**) and $N = 3$ (**d**) vPCB specimens. **e**, Flammability test of vPCB. The sample is retracted after 0 s to move it away from the burner.

Moisture absorption of GFRV is characterized through immersion in water according to the IPC PCB standard (see Methods for details). Figure 2e shows that our vitrimer is on par with common PCB dielectrics such as polyimide and within 0.2% of FR-4. We hypothesize that the difference is due to the presence of ester linkages between monomers and could be further reduced by modifying the vitrimer chemistry. Flexural strength is also evaluated using a three-point flexural test (see Methods) and the results are visualized in Fig. 2f. The performance is within the range of FR-4-based materials, and these values could be tuned by changing the quality of the glass fibre weave.

Vitrimer-based PCB

We create ‘recyclable’, ‘reusable’ and ‘repairable’ circuit boards by integrating vitrimer materials into PCBs. The first step to creating a PCB from raw GFRV is adding a conductive copper layer. In traditional

PCB manufacturing, a glass fibre weave is impregnated with an epoxy resin and partially cured. The resulting material, known as prepreg, is laminated with copper foil and can be patterned and stacked to create multilayer circuits. We use a similar lamination process illustrated in Fig. 3a. Sheets of copper foil are laminated on the raw GFRV in a heat press (see Methods for details). This method can scale to roll-to-roll manufacturing for high-volume production.

To assess copper adhesion, the peel strength for 16 copper-clad laminates (CCLs) is systematically measured for heat-press temperatures of 120–160 °C and heat-press time of 30 min to 2 h. Our results show that adhesion between the copper and vitrimer increases as the heat-press temperature and time increase (Fig. 3b). We note however that above 180 °C, lower viscosity causes the vitrimer to be squeezed out. The results follow the expected trend, whereby the increase in temperature and pressure results in dissociation in the CAN, thereby

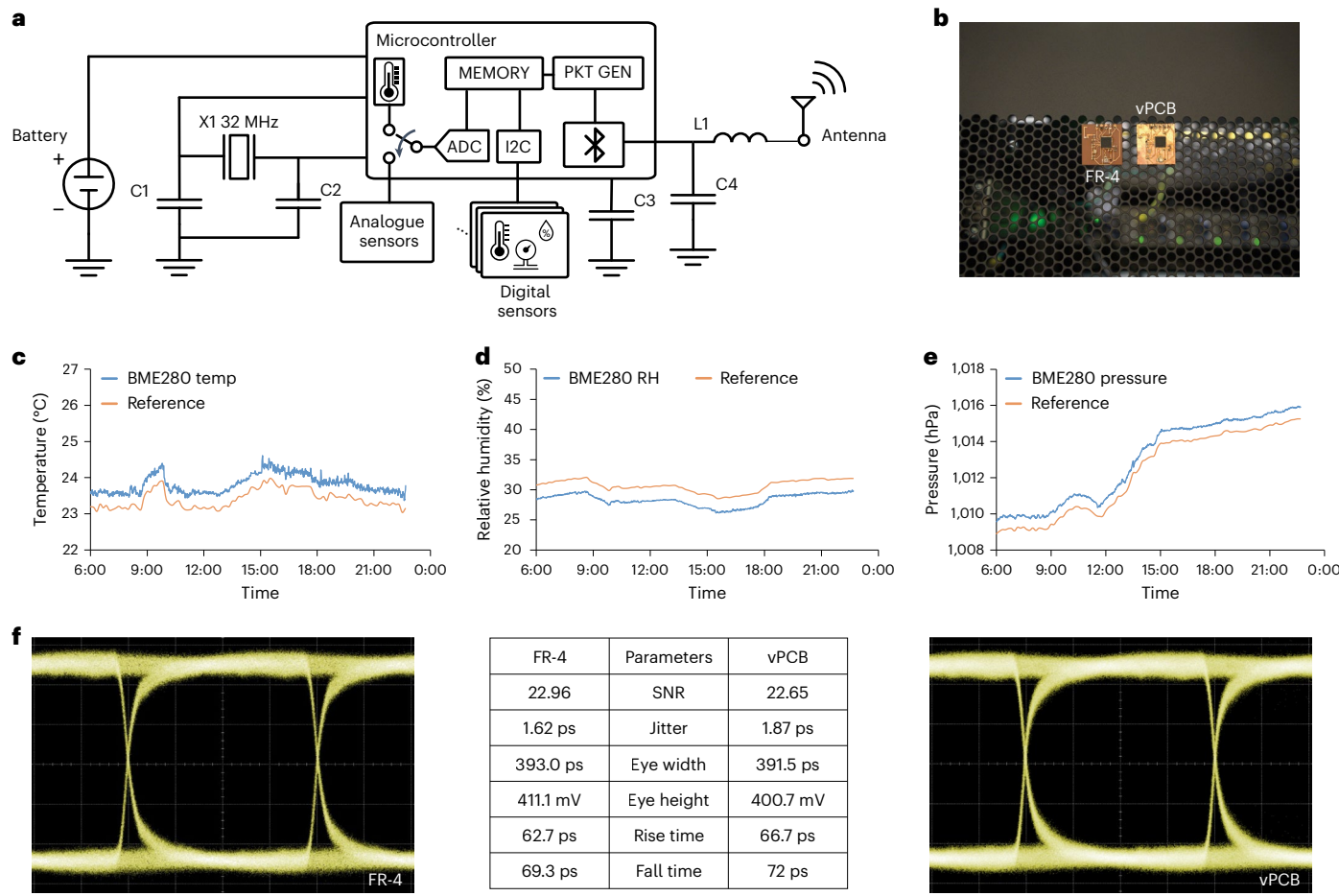


Fig. 4 | Platform evaluation. **a**, Circuit block diagram. ADC, analogue-to-digital converter; PKT GEN, packet generation; C1–C2, capacitor 1–capacitor 2; L1, inductor 1; X1, 32 MHz crystal oscillator 1; I₂C, inter-integrated circuit. **b**, Photograph of the experimental setup. **c–e**, Data centre temperature (**c**),

relative humidity (**d**) and pressure (**e**) measurements from two platforms over 16 h showing successful continuous running and high-frequency signal transmission. **f**, Comparison of eye diagrams of FR-4 and vPCB.

increasing the availability of reactive sites for adhesion. Bonding can be further improved by adding a thin, partially cured vitrimer layer between the GFRV and the copper foil. This significantly enhances peel strength after thermal stress, exceeding the PCB standard (Extended Data Fig. 2), as the partially cured vitrimer has more reactive sites available.

Next, circuit traces are patterned onto the copper-coated substrate. Chemical etching and laser structuring are two commonly used processes in PCB manufacturing. We demonstrate compatibility with both processes. Briefly, the raw copper-coated GFRV is placed in a laser micromachining system (LPKF Protolaser U4), which drills holes and directly removes copper to pattern circuit traces. Alternatively, we can coat the copper with a thin mask layer, use the laser to selectively remove the mask, then place the board in a ferric chloride solution to etch away exposed copper. These methods can pattern individual layers that can be aligned and heat pressed to create a multilayer laminate. The final step is applying a mask layer and using electroless copper plating to connect the layers through vias (see Methods for details).

We compare vPCBs to traditional FR-4-based circuits. The dielectric constant and loss tangent of the PCB are critical for high-frequency electrical signal integrity. The dielectric constant and loss tangent of our vPCB compared to various FR-4 types are shown in Fig. 3c,d, respectively (see Methods for procedure). The results show that our vPCB's dielectric constant is within the typical specification range of 3.5–5.5. This value can be tuned by changing the glass fibre volume content, vitrimer chemistry and polymer-free volume.

Low flammability is another crucial property required to protect PCBs from potential ignition as many electronics produce heat.

Conventional FR-4 PCBs are formulated with flame retardants to self-extinguish fires. We evaluate the flammability of vPCB. The fire was extinguished within 7 s after removing the flame source (Fig. 3e and Supplementary Video 2), conforming to the 10 s standard.

Platform evaluation

To evaluate the potential of vPCBs, we prototype an IoT sensor to monitor temperature, humidity and pressure. Such sensors provide critical information for environmental and smart-building monitoring, and this industry is projected to grow by billions of new devices which raises a pressing need to mitigate their environmental harms³⁶. In addition, a complete IoT sensor must perform all the basic functions of a small computer and transmit radio signals at GHz frequencies, which are affected by a PCB's properties such as dielectric constant and loss tangent. Our prototype includes a microcontroller with a Bluetooth radio, a sensor, battery, onboard antenna and passive components as shown in Fig. 4a (see Methods for details). We fabricate identical circuits on vPCB and standard FR-4, and programme both to wirelessly transmit sensor measurements from a data centre setting for 16 h as shown in Fig. 4b. Figure 4c–e show the resulting measurements. Both devices successfully transmitted Bluetooth packets with no data gaps or device failures. The sensor data are closely correlated, but with small fixed offsets probably due to individual sensor variation or their small physical separation.

Next, we perform eye diagram measurements to characterize digital transmission metrics such as signal-to-noise ratio (SNR) and clock jitter. A well-routed signal line is patterned onto vPCB and FR-4.

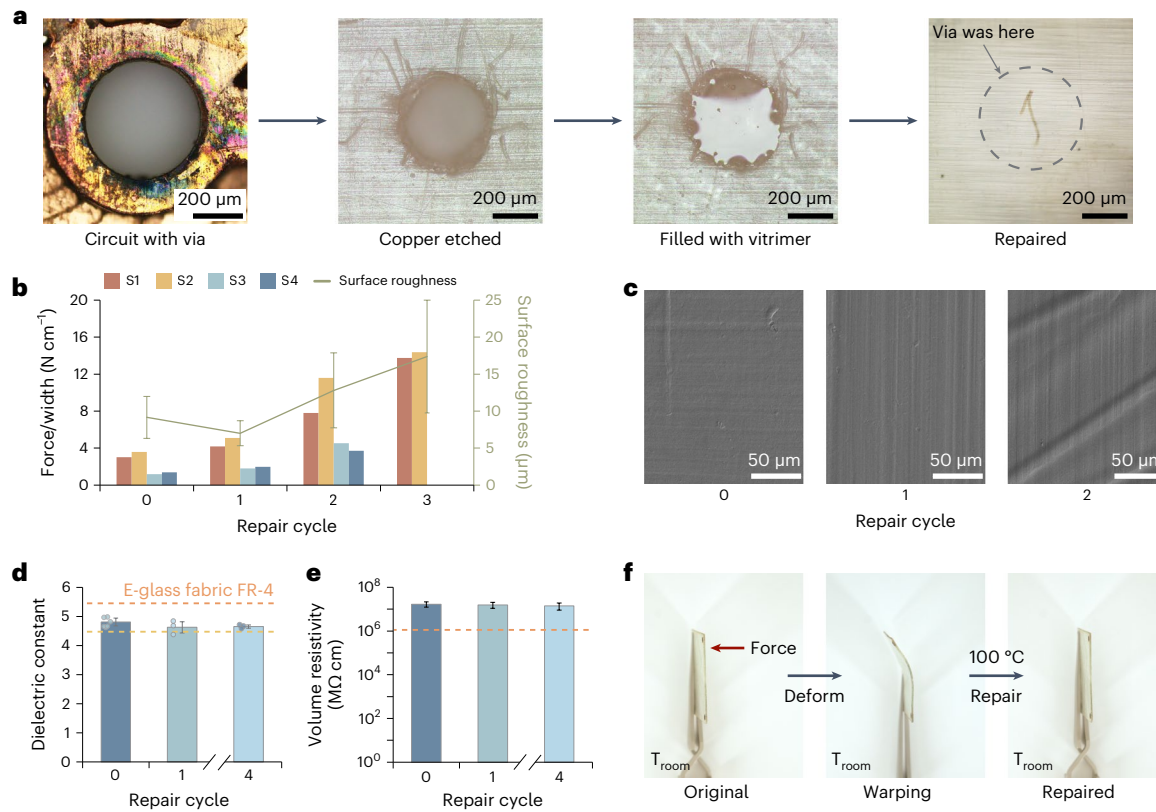


Fig. 5 | Repair and remanufacturing of vPCB. **a**, Optical micrographs of a via on vPCB being healed. **b**, Average peeling force of copper-clad laminates after three repair cycles for various specimens, with secondary vertical axes showing the corresponding surface roughness before each repair cycle (data are mean \pm s.d. of 3 vPCB specimens). **c**, SEM images of GFRV surface after each repair cycle, showing orderly indentations caused by heat-pressed copper foil. **d,e**, Characterized dielectric constants (**d**), and volume resistivities (**e**) of repaired GFRV after each repair cycle compared to the PCB standards of woven

glass FR-4 (yellow dashed line) and e-glass fabric FR-4 (orange dashed line); data are mean \pm s.d. of 3 vPCB specimens in **1(d)** and 1,000 (**e**) measurements. Remanufactured vPCB exhibits nearly identical dielectric constants and volume resistivities. **f**, Thermadapt shape-memory behaviour of GFRV. GFRV is deformed under external force and is recovered to its original shape after being heated at 100 °C for 1 min. This allows for the repair of warped vPCBs at elevated temperatures, making it a more environmentally friendly option compared with traditional PCBs.

We measure the eye diagram of a 2.48 Gb s⁻¹ pseudorandom binary sequence from a serial BERT (Keysight N4903A) using an oscilloscope (Keysight 86100D) and find nearly identical performance (Fig. 4f).

Repair and remanufacturing

A unique property of our vPCBs is that the vitrimer's dynamic CANs enable the healing of physical damage such as fractures and holes. This enables repairing and remanufacturing of PCBs to reduce their environmental impact. A recent study from Microsoft³⁷ showed that repairing broken devices improved greenhouse gas emissions and waste avoidance by 85% and 90%, respectively, compared with replacing the whole device. Once devices are beyond repair, we explore using vPCBs to enable value cycling by repairing damaged base materials and remanufacturing them.

A repair method that heals holes and fractures is developed as shown in Fig. 5a. Copper is first removed through chemical etching. Subsequently, the holes are filled with a small amount of fresh liquid vitrimer. We follow the heat-press process in Fig. 2b to create a new CCL. The repaired GFRV is shown in Fig. 5a, wherein all the holes have been healed and are no longer visible. The joint strength of healed holes is also evaluated using a shear punch test (see Methods and Extended Data Fig. 3). In comparison with repairing FR-4 with cyanoacrylate glue, the vitrimer creates a stronger bond at the hole boundary, avoiding catastrophic failure as seen with the super glue. The healing capability of vitrimer chemistries enables the creation of new covalent bonds between fresh vitrimer and GFRV. Specifically, the transesterification reaction occurring in the vitrimer system

leads to topological rearrangements while preserving the integrity of the molecular network^{27,38}. This healing mechanism cannot be achieved by traditional thermoplastics or thermosets. Using the same fabrication steps above, we can use the resulting bare GFRV to create new circuits.

We evaluate copper adhesion after four repair cycles of copper re-lamination as shown in Fig. 5b. We find that the interfacial adhesion improves after each cycle. This is probably attributed to the microscale indentations on the GFRV surface caused by heat-pressed copper foil, as observed using scanning electron microscopy (SEM) shown in Fig. 5c. These indentations increase the surface roughness after each remanufacturing attempt, which is known to improve adhesion³⁹. The dielectric constant and volume resistivity of the repaired material remain within the range of common FR-4, varying by a maximum of 6.5% even after four repair cycles as shown in Fig. 5d,e.

vPCBs also have shape-memory properties that can be used to reverse physical damage that can occur due to mechanical stress such as graphics processing unit sagging. Mechanical deformation of the vPCB below its vitrimer transition temperature (T_v) results in a temporary shape change. Subsequent heat treatment at 100 °C (above both T_g and T_v) for 1 min prompts the material to revert back to its original pre-deformation configuration. Figure 5f demonstrates a GFRV that has been deformed under an external force, then successfully recovers to its thermodynamically favoured original shape after heat treatment. This shape-memory attribute underscores the self-healing properties of vitrimers and highlights the potential for the circular reuse of mechanically damaged vPCB materials.

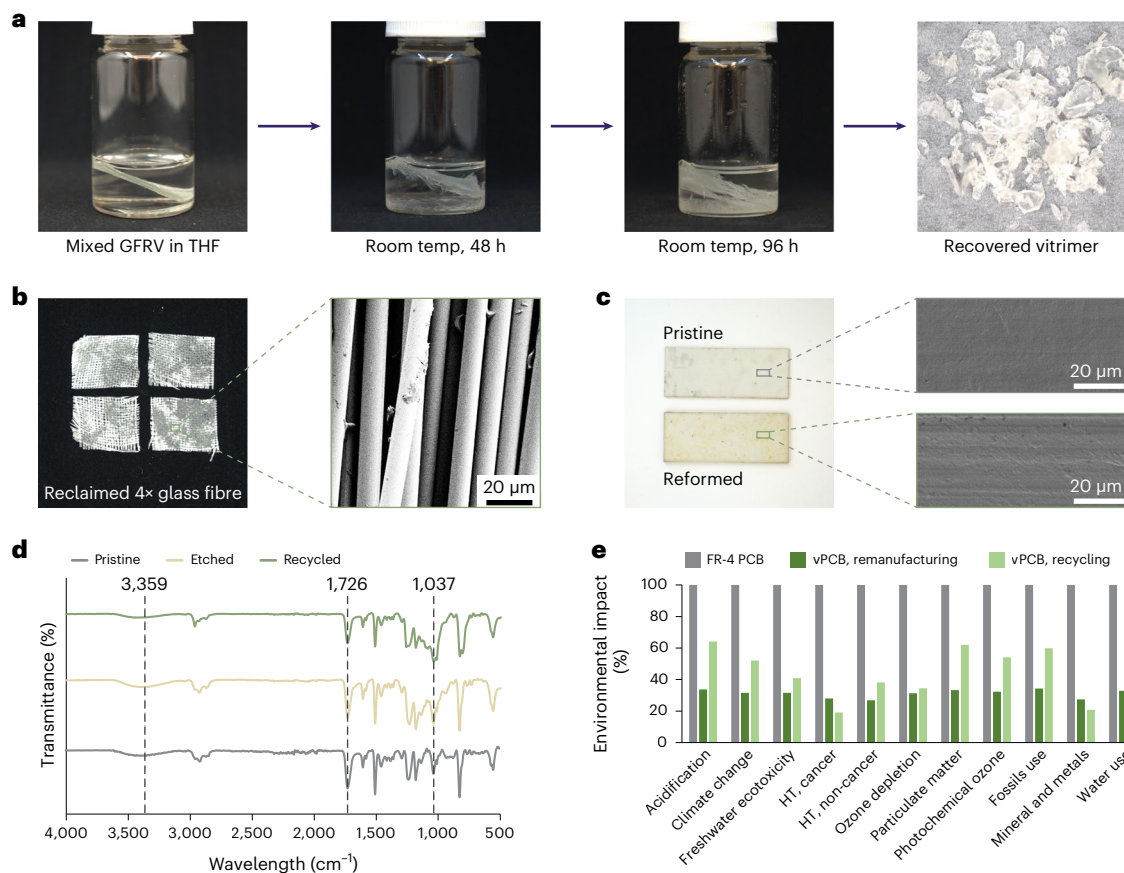


Fig. 6 | Recycling of vPCB. **a**, Photographs showing recycling procedures of GFRV from an obsolete PCB and recovered vitrimer matrix after precipitation from the THF. **b**, Photograph of reclaimed glass fibre weaves and SEM image showing the clean microstructure from recycling. **c**, The recovered vitrimer was reused to form new GFRVs. The appearance of the reformed sample remains nearly identical to the pristine sample, and SEM images show smooth surfaces of reformed GFRV without any microcracks or pores. **d**, Comparison of FTIR spectra

of pristine vitrimer, vitrimer after etching and recovered vitrimer from THF. **e**, Environmental impact comparison of conventional FR-4 PCB and vPCB in end-of-life disposal scenarios across 11 different categories. vPCB is assumed to have four cycles of remanufacturing or recycling, with a THF recovery efficiency of 97% in the recycling scenario. As a comparison baseline, FR-4 PCB is assumed to have 5 lifetimes with the best-case assumption for end-of-life incineration of each board. The vPCB results are normalized to the FR-4 PCB for each category.

Closed-loop recycling

Vitrimer-based PCBs can be repeatedly repaired through the process described above; however, these PCBs will eventually reach end-of-life when a design becomes outdated or if repair is no longer economically feasible. To maximize circularity, we develop a closed-loop recycling process for end-of-life vPCBs to non-destructively disassemble the fibre composites into high-quality raw materials for use in new, fully functional circuit boards.

We begin the vPCB recycling processes by removing the components, cleaning the surface and then dissolving the copper using ferric chloride to isolate the GFRV substrate (see Methods for details). Figure 6a illustrates our process for deconstructing the GFRV into raw materials. We immerse the GFRV sample in various polar aprotic solvents to extract glass fibres. We examined acetone, chloroform, dimethylformamide (DMF) and tetrahydrofuran (THF). We found that DMF and THF do not react with the GFRV materials, but their small molecules can ingress into the polymeric network, resulting in swelling (Extended Data Fig. 4 and Supplementary Video 1). This swelling enables the separation of the vitrimer matrix and glass fibres without chemical degradation. We select THF for our recycling process, as it achieves similar swelling performance but has a low boiling point of 66 °C and enables easy solvent removal to recover the vitrimer. In contrast, DMF has a higher boiling point of 153 °C and requires rotary evaporation which may result in the loss of the catalyst in the material (see Supplementary Information 1.1).

The vitrimer matrix is fully separated from the glass fibre layers after immersion in THF for 96 h (shown in Fig. 6a, details in Methods). The recovered vitrimer and glass fibre are shown in Fig. 6a,b, respectively, and can be reused directly after drying. Vitrimer polymer can be easily recovered with ~98% isolated yield after being precipitated out from the THF, and 100% of the glass fibre is recovered. We also demonstrate a THF recovery efficiency of ~91%, with 1.5% evaporation loss during testing and measurements, and 7.5% remaining in the swollen vitrimer matrix that we did not attempt to recapture. The THF recovery efficiency could be further optimized to over 97% by performing recycling in a properly designed and operated recovery system⁴⁰. This is a marked improvement over previous solvolysis methods, which necessitate additional adsorption or distillation procedures to remove the solvent and recover the polymer matrix.

We create new GFRV samples using recycled materials by grinding the recovered vitrimer into a fine powder, mixing it with a 40 wt% fresh vitrimer in viscous liquid form to fully penetrate the small interspaces in our dense glass fibre weave, and applying the same heat-press process above. We note that the required pressure has an inverse quartic relationship to pore size according to the Hagen Poiseuille equation, suggesting the potential for using 100% recycled vitrimer by adjusting the material or process parameters (see Supplementary Information 1.2). The resulting reformed GFRV is shown next to a newly made GFRV sample in Fig. 6c. The resulting composite showed no apparent differences except for slight discoloration on the surface due to thermal oxidation.

We hypothesize above that small-molecule solvent-based swelling does not degrade the materials; however, this method raises multiple fundamental questions of whether the process removes non-covalently bonded catalyst critical to the transesterification vitrimer's properties, whether it affects the crosslink density, or changes the polymer backbone. We first examine SEM images of reformed GFRV, which show smooth surfaces without any noticeable damage in the form of microcracks or pores (Fig. 6c). At a macro scale, this confirms that the dynamic nature of the polymeric macromolecular network is preserved after every recycling as the polymer can flow and form a continuous sheet from pulverized recycled vitrimer powder without being disassociated by the solvent.

The mechanical behaviour of the recycled vitrimer matrix is evaluated by comparing the storage modulus and tan delta values post-recycling (Extended Data Fig. 5a,b). We quantify the retention of storage modulus post-recycling, observing 96.9% after recycling once and 94.4% after two cycles (Extended Data Fig. 5c). Although we observe some narrowing and broadening of the tan delta peak between cycles (see Supplementary Information 1.3), the high storage modulus retention indicates that the reduction in crosslink density from recycling is negligible. To evaluate the potential loss of non-covalently attached catalyst during our recycling procedure, we leveraged Maxwell's relation for viscoelastic materials to derive Arrhenius curves⁴¹ (Extended Data Fig. 5d). We determined a T_g of 79.6 °C for pristine vitrimer. Upon recycling once, the T_g was slightly reduced to 78.3 °C and 79.4 °C after recycling twice. The marginal shift in T_g implies no loss of the non-covalently bonded catalyst throughout our THF swelling recycling process across multiple cycles, as a reduction in catalyst concentration within the vitrimer would precipitate a substantial increase in T_g ⁴¹.

To further verify the chemical composition of the vitrimer polymer backbone at different recycling stages, we use Fourier-transform infrared (FTIR) spectroscopy and compare results against a new GFRV sample in Fig. 6e. We observe the disappearance of 903 cm⁻¹ for the epoxy functional group after the vitrimer is cured, and the appearance of sharp peaks at 1,037 cm⁻¹, 1,726 cm⁻¹ and broad intense peaks at 3,359 cm⁻¹ for -CO-O-, -C=O and -OH groups, respectively. This indicates the consumption of all epoxy end groups for the formation of ester linkages with crosslinked networks in vitrimers. The recovered vitrimer retained identical functional groups with characteristic peaks as the original, as shown in Fig. 6d. This indicates that recycled vitrimers maintain their crosslink density and undergo exchange reactions without changing the chemical polymer backbone. Figure 6e also indicates that the vitrimer can resist ferric chloride corrosion, which enables the production of vPCBs through the conventional and scalable PCB manufacturing technique of chemical etching. The properties of GFRV made of recycled vitrimer are also highly comparable to the original (Extended Data Fig. 6).

Life-cycle assessment

We perform an LCA⁴² to evaluate the environmental impact of our vPCB and compare our remanufacturing and recycling processes to conventional PCB fabrication and disposal at scale. Our cradle-to-cradle LCA uses industrial models and encompasses material synthesis, CCL manufacturing, freight transportation and end-of-life PCB disposal or recycling.

Notably, our GFRVs are 'cured' laminates. This is a key advantage over conventional prepreg materials which have limited shelf lives of 3–6 months⁴³. Maximizing prepreg lifetimes requires refrigeration and low-humidity environments, thereby increasing their environmental footprint. We compared the environmental impact of vPCB freight with FR-4 preprints. The LCA demonstrates a substantial reduction of 20.0% in GWP, 28.0% in ozone depletion potential, 14.0% in fossil fuel depletion and 26.0% in mineral and metal use (Extended Data Fig. 7).

To compare vPCBs with conventional PCBs in end-of-life scenarios, we use the business-as-usual standard of incineration as the baseline. Our model makes the best-case assumption for conventional PCBs, where 89.3% of the waste heat and 11.1% of the waste electricity are recovered and credited as energy production. Our remanufacturing scenario models product repair and our LCA looks specifically at the environmental cost of remanufacturing the PCB using the methods above. In the recycling scenario, the product is broken down into raw materials that are used to create new PCBs.

The results shown in Fig. 6e indicate that vPCBs could substantially reduce environmental impacts including acidification, GWP and ozone depletion potential. Extended Data Fig. 8 shows a detailed breakdown of the carbon footprint of a conventional PCB indicating that raw materials make up 48.5%. We show that vPCBs enable remanufacturing with substantially less material and energy, and with potential for multiple cycles to further reduce impact. Our LCA indicates reductions of over 65% in all metrics with four remanufacturing cycles.

The primary benefits of using vPCBs are reducing end-of-life by-products, disassembling end-of-life vPCBs into raw materials and creating new, fully functional circuit boards. Four recycling cycles show a reduction in 11 metrics of up to 80.9%. This includes a 35.8% reduction in acidification, 47.9% in GWP, 59.1% in freshwater ecotoxicity, 61.8% in human non-cancer toxicity emissions, 65.5% in ozone depletion potential, 38.0% in particulate matter, 45.9% in photochemical ozone, 40.2% in fossil fuels depletion, 79.2% in mineral and metals use, and 28.1% reduction in water use. Notably, vPCBs could reduce human cancer toxicity emissions by 80.9%.

Discussion

We report a recyclable PCB based on transesterification vitrimers and a non-destructive, swelling-based separation method to recycle them. The ubiquity of circuit boards enables the potential for widespread use of vPCBs from consumer devices to industrial and medical equipment. We optimize our recyclable PCB formulation to achieve electrical and mechanical properties on par with conventional PCBs and compatibility with current EMS ecosystems to make vPCBs near drop-in replacements for FR-4.

Net zero emissions and reducing environmental waste have become a global mission. The repairability and closed-loop recyclability of vPCBs both reduce toxic by-products and improve a broad range of environmental impact metrics. We demonstrate vPCBs as a choice for companies and industries prioritizing sustainability and environmental consciousness. In addition, the abundance and widespread availability of epoxies and catalysts create opportunities to design vPCBs optimized for specific properties. Our approach of swelling PCBs could also be explored for other composite materials and automated disassembly of circuit components to enhance value recovery from ICs during recycling. We hope this study opens new directions for recyclable materials and composites for the electronics and computer industry centred around environmental sustainability.

Methods

Vitrimer chemistry selection

We focused this work on developing a recycling process rather than developing a vitrimer chemistry. We optimized for similarity to conventional FR-4 by choosing a high-performance chemistry demonstrated in previous work⁴⁴ using the same bisphenol-A epoxides typically used in conventional FR-4 (ref. 31) and which are available at low cost. We note that while this is a petroleum-based material, our proposed recycling process reuses the entirety of the polymeric matrix, thereby eliminating any BPA waste. In addition, the proposed recycling method is based on the fundamental behaviour of the vitrimer macromolecular network and may be expected to adapt readily to alternative vitrimer formulations. Our vitrimer swelling-based recycling approach

opens up new avenues for future investigation of this method for novel non-petroleum-based vitrimers⁴⁵.

Fabrication of GFRV composite

The GFRV composite was constructed from two parts: vitrimer polymer and woven glass fibre sheets. The vitrimer polymer was prepared by mixing a stoichiometric ratio (1:1.5 mol% to the acid) of epoxy (EPON 828, Skygeek), adipic acid (Sigma Aldrich) and 1,5,7-triazabicyclo[4.4.0]dec-5-ene (TBD, Sigma Aldrich). The epoxy was poured into a beaker, then placed in a 100 °C heated bath and stirred at 100 r.p.m. for 10 min. The beaker was kept in the heated bath for the remainder of the mixing process. Subsequently, transesterification catalyst TBD was added into the beaker and stirred at 600 r.p.m. for 5 min to thoroughly blend the epoxy and fully incorporate the catalyst into the mixture. Adipic acid was added last and stirred for an additional 7 min to ensure a homogeneous mixture. The beaker containing the mixture was then placed into a vacuum for 2 min for degassing.

Glass fibre (0/90, 2 oz fibreglass fabric, Fibre Glast) was cut to size and stacked into a metal mould cavity. The mould was then left in a vacuum oven to preheat at 140 °C for 20 min. The treated mixture was then rapidly cast into the mould, followed by 1 min of degassing to eliminate air from the mould cavity and the matrix. The mould was then placed in a compression moulding heat press (Carver 5420) for 7 h with a constant temperature of 160 °C for thermal curing. A constant pressure of 1 MPa was applied to the mould for the first 5 h, and 4 MPa was applied for the last 2 h for post-curing. To avoid adhesion between GFRV and the metal mould, a sheet of PTFE was placed on the mould's cavity plate and the core plate at the beginning of each fabrication process. After the thermal curing and mould cooling, the resulting GFRV of overall dimension 75 × 75 × 0.5 mm was collected and stored in a desiccant chamber for further characterization and manufacturing. We note that the size of the samples is due to the mould used and the same method could be scaled for larger samples.

vPCB manufacturing

We describe the manufacturing process for creating circuits on our vPCB below. To start the process, the surface was treated and copper was laminated onto GFRV. Subtractive patterning methods were then utilized to create circuit traces. Each step is described in detail below.

Lamination. Two 25-μm-thick sheets of copper foil (1 oz, McMaster-Carr) were first laser cut to the appropriate size and placed on both sides of GFRV. Subsequently, the laminate was placed in an aluminum mould and sandwiched between two layers of load spreader with alignment pins at the four corners. The structure of the layup in the heat press is schematically illustrated in Supplementary Fig. 5. Then the mould was heat pressed at 160 °C and 2 MPa for 2 h.

Printing circuit design. To ensure proper alignment of the laminate during the PCB design process, the four alignment holes that were previously drilled for lamination were utilized. An important feature of multilevel PCBs are vias, copper-plated holes drilled through the board that provide electrical connections between different copper layers. To create vias, through holes were first drilled in the desired positions on the laminate using either a CNC machine (Nomad 883 Pro) or a laser (LPKF ProtoLaser U4). For the CNC, a rotational speed of 10,000 r.p.m. and a feed rate of 6 inch min⁻¹ were selected; for the laser, frequency, power, mark speed, number of repetitions and delay were set to 50 kHz, 1.5 W, 250 mm s⁻¹, 10 repetitions and 1,000 ms, respectively.

Next, copper was deposited onto the inner surface of the holes using electroless plating. To do this, a mask (Semiconductor Equipment) was first applied to completely cover the surface of the copper layers and the sides of the laminate, with openings in the via holes to allow for copper deposition. Once the mask had been applied, the

following steps were applied for electroless plating. The laminate was first immersed in 10 ml 3% SnCl₂ solution with 2% hydrochloric acid and 95% H₂O (Caswell) for 2 min to sensitize the via walls. This was followed by immersion in a 10 ml 3% PdCl₂ solution with 2% hydrochloric acid and 95% H₂O (Caswell) for 2 min to activate the substrate surface for subsequent plating. Notably, the laminate was rinsed with distilled water between each step to ensure the complete removal of unwanted ions. Finally, the laminate was immersed in a 20 ml solution of 5% copper(II) sulfate pentahydrate (Caswell) at room temperature for 60 min to deposit copper onto the vias. After plating, the mask was removed and the laminate was rinsed with distilled water.

Lastly, we patterned the circuit traces. Laser structuring is often used for more intricate circuits due to its high precision, ability to cut through a wider range of materials and speed in small-scale manufacturing. Chemical etching is less precise but is more suited for low-cost, large-scale production because it can etch many parts or multiple boards simultaneously. For the laser process, a laser micromachining system (LPKF ProtoLaser U4) was used that scans its beam across the surface and removes the copper. The laser parameters were carefully tuned to minimize heat-induced carbonization to the vitrimer surface. The specific parameter settings are shown in Supplementary Table 1. For the chemical etching process, the copper was coated in a mask material and patterned with the laser to remove the mask outside the desired copper traces. The board was then immersed in 40% ferric chloride (M.G. Chemicals) at room temperature for 20 min. After all the unprotected copper had been etched, the mask was removed and the board rinsed with distilled water.

Recycling

All the components on the PCB were removed following the PCB rework standard IPC-7711 (Procedure 3.3.3)⁴⁶. After desoldering all the components, the vPCBs underwent a cleaning protocol to ensure the removal of dust and other surface contaminants through isopropyl alcohol (IPA) rinses and high-pressure air jets. It is noteworthy that in industry, PCBs typically undergo rigorous cleaning processes after manufacturing. These processes include ultrasonic cleaning, gas phase cleaning and deionized water washing. The same cleaning techniques can be applied to scale up the cleaning process before vPCB recycling.

Subsequently, the PCB with copper tracks was immersed in ferric chloride at room temperature for 1 h to etch all the copper. Soldering pastes were precipitated after all the copper has been dissolved, and they were reclaimed through simple filtration (Supplementary Fig. 2).

Once the copper was removed, the remaining GFRV was immersed into THF (186562 tetrahydrofuran, Sigma Aldrich), then kept at room temperature for 96 h without disturbance. We repeated this process at 40 °C and observed that it could be expedited to 24 h by heating THF up to 40 °C, as heat increases the swelling rate of the vitrimer matrix.

After the separation of the vitrimer matrix and glass fibres, they were collected from THF and kept in a vacuum oven for 24 h to evaporate any residual THF. The recovery yield of the vitrimer polymer and glass fibre was calculated by dividing the weight of the recovered vitrimer and glass fibre, after precipitation from the THF and drying, by the weight of the respective materials before undergoing the recycling process. Afterwards, the recovered vitrimer was pulverized into powder form using a cutting mill (Eberbach E3300). The resulting vitrimer powder and reclaimed glass fibres were then ready to be reused for the fabrication of a new GFRV.

Electrical characterization

Dielectric constant. The dielectric constant test was conducted using a vector network analyser (VNA, Anritsu MS2036C) following the standard PCB test method IPC-TM-650 (Method 2.5.5.6) full sheet resonance (FSR) test⁴⁷. Test specimens were CCLs trimmed accurately to a rectangular shape with dimensions 29 × 29 × 0.47 ± 0.12 mm. An SMA connector was used to connect the specimen to a VNA S11 port with the signal pin of the SMA connector soldered to one side of the copper

layer of the laminate and the ground pins soldered to the other side. The capacitance of the parallel plate was measured at a frequency of 1 MHz, with the ambient temperature during the test set to be in the range of 22 °C to 24 °C. The dielectric constant of the vitrimer was determined using the following formula: $k = CT/\epsilon_0 A$, where C is the capacitance reading from the VNA, T is the effective thickness of the specimen, ϵ_0 is the vacuum permittivity and A is the area of the specimen.

Resistivity. Volume resistivity tests were conducted using a sourcemeter (Keithley 2470). CCLs with dimensions $29 \times 29 \times 0.6 \pm 0.05$ mm were prepared as test specimens. The volume resistance was measured by connecting a sourcemeter test lead to each side of the laminate. The current was measured while applying 40 V DC across the specimen. The ambient temperature was maintained at 25 °C during the interval when electrical measurements were being made. The volume resistivity of the vitrimer was calculated using the formula: $r = RA/T$, where R is the measured resistance, A is the effective area of the surface and T is the average thickness of the specimen.

Mechanical characterization

Dynamic mechanical analysis. Dynamic mechanical analysis (DMA) was conducted using an Electroforce 3200 (TA Instruments). Rectangular coupons with dimensions of $30 \times 6 \times 0.5$ mm were laser cut from the vitrimer sheets. Stress-relaxation tests were done using 4% initial strain with dwell time of 4,000 s at different temperatures ranging from 140 °C to 240 °C. The stress-relaxation constant (τ) was calculated for each temperature using the stress–time curve, and these values were plotted on $\ln(\tau)$ vs inverse of temperature to calculate T_g . Non-isothermal DMA experiments were done using scanning temperatures ranging from 20 °C to 120 °C at a frequency of 1 Hz, resulting in corresponding storage modulus (E'), loss modulus (E'') and tangent of delta ($\tan \delta$) curves for each scan.

Peel strength. To measure the bond strength between the copper layer and the dielectric material, that is, GFRV, peel strength tests were conducted on an Instron load frame (Instron 5585H) following the standard PCB test method IPC-TM-650 (Method 2.4.8.1)⁴⁷. Samples with different heat-press times and temperatures were compared, while other variables remained consistent during the manufacturing process. Specimens with dimensions of 29×29 mm with two 20-mm-width test strips were peeled, the peel angle was fixed at 180°, and force was applied in the vertical direction at a speed rate of 50 mm min⁻¹ (until the peel was completed). The testing setup is schematically illustrated in Supplementary Fig. 6.

Flexural strength. Flexural strength test was conducted on an Instron load frame (Instron 5585H) in accordance with IPC-TM-650 Method 2.4.4 (ref. ⁴⁷). GFRVs with dimensions of $60 \times 25 \times 0.51$ mm were prepared as test specimens. Specimens were centred on the span supports with the long axis perpendicular to the crosshead, with a bending span of 25.4 mm. The testing setup is shown in Supplementary Fig. 7. The test was performed under ambient conditions, and the load was applied at a constant rate of crosshead movement of 0.76 mm min⁻¹. Flexural strength was calculated using the formula: $S = 3PL/2WH$, where P is the loading at breaking, L is the span, and W and H are the width and thickness of the specimen, respectively.

Joint strength. Joint strength test was conducted on an Instron load frame (Instron 5585H). GFRV and FR-4 with dimensions of $29 \times 29 \times 0.6$ mm were prepared as test specimens. Circles with a diameter of 10 mm were laser cut from the specimens. The holes in the GFRV were repaired with fresh vitrimer, while the holes in the FR-4 were repaired using super glue (Insta-Cure+, Bob Smith Industries) along with additional FR-4 circles that were also laser cut to a diameter of

10 mm to ensure a stiff interfacial strength and prevent any deformation of the repaired holes in FR-4 during testing. Specimens were centred on a hollow metal cylinder support with the long axis perpendicular to the punch, with a support span of 16 mm. The testing setup is illustrated in Extended Data Fig. 3a. The test was performed under ambient conditions, and the load was applied at a constant rate of punch movement of 0.1 mm per min. Joint strength was calculated using the formula: $\tau = F/\pi dh$, where F is the loading at breaking, and d and h are the diameter and thickness of the hole, respectively.

Chemical characterization

Moisture absorption. Moisture absorption of GFRVs was evaluated following IPC-TM-650 Method 2.6.2.1 (ref. ⁴⁷). A specimen measuring $29 \times 29 \times 0.51$ mm with sanded edges was first dried in an oven at 100 °C for 1 h, cooled to room temperature in a desiccator and weighed immediately upon removal from the desiccator. Subsequently, it was immersed in a glass container filled with distilled water kept at 23 °C in a fume hood. The specimen was collected from the water after 24 h, dried with Kimwipes and an air blow gun, and weighed immediately to determine the final weight. Moisture absorption was calculated as the percent increase in weight: $100\% \times (\text{final weight} - \text{initial weight})/\text{initial weight}$. The testing setup is shown in Supplementary Fig. 8.

Flammability. Flammability of GFRVs was evaluated in accordance with IPC-TM-650 Method 2.3.10 (ref. ⁴⁷). GFRV samples with dimensions of $60 \times 12.5 \times 0.54$ mm were first exposed to standard laboratory conditions for 24 h. Subsequently, the burner was safely placed in a fume hood, and then ignited and adjusted to produce a blue flame 19 mm high. The specimen was mounted in the test fixture with its longitudinal axis vertical, and placed centrally above the blue flame. The burner was withdrawn from the specimen after 10 s. The testing was recorded on video (Supplementary Video 2), and the burning duration was calculated using frames in seconds.

Wireless IoT prototype

To demonstrate the potential applications of our vPCB, an IoT platform that features wireless communication and functional control, signal reading and transmission was designed around the BLE-integrated nRF52 SoC (nRF52832, Nordic). Visual Studio Code with Arduino extension was used for microcontroller unit programming. A Bluefruit Connect Android application was used for communication between the microcontroller and mobile devices. Sensor measurements were read either using the microcontroller's analogue-to-digital converter (ADC) for analogue sensors, or by sending a command using the standard I²C serial communication bus to read digital data from various external sensors. The operation of temperature, humidity and pressure sensing was demonstrated (BME280, Bosch Sensortec). Sensor data were then transmitted via Bluetooth.

Life-cycle assessment

Our modelling system encompasses the entire life cycle of vPCB, from raw material extraction and manufacturing to end-of-life disposal, with typical use case assumptions made for factors such as the 1.7% surface area of via holes in a PCB, 10% loss of glass fibre due to fraying, 97% recovery efficiency for THF, as well as waste management. All other variables that determine the amount of material and energy needed for remanufacturing and recycling scenarios were collected in the lab testing environments to provide accurate information for the life-cycle inventory, including raw material recovery percentages, water usage and energy consumption.

All background unit process inventories were derived from the Ecoinvent database and implemented in the LCA software GaBi, adopting the EF method (v.3.0) for impact assessment of the environmental footprint initiative.

Reporting summary

Further information on research design is available in the Nature Portfolio Reporting Summary linked to this article.

Data availability

All data needed to evaluate the conclusions of this study are available in the paper or in the Extended Data and Supplementary Information. Source data are provided with this paper.

Code availability

The source code is available for download on GitHub at <https://github.com/iamZhihanZhang/vPCB-IoT-Platform.git>.

References

1. Hibbert, K. & Ogunseitan, O. A. Risks of toxic ash from artisanal mining of discarded cellphones. *J. Hazard. Mater.* **278**, 1–7 (2014).
2. Awasthi, A. K., Zeng, X. & Li, J. Environmental pollution of electronic waste recycling in India: a critical review. *Environ. Pollut.* **211**, 259–270 (2016).
3. Song, Q., Li, J. & Zeng, X. Minimizing the increasing solid waste through zero waste strategy. *J. Clean. Prod.* **104**, 199–210 (2015).
4. Forti, V., Balde, C. P., Kuehr, R. & Bel, G. *The Global E-Waste Monitor 2020: Quantities, Flows and the Circular Economy Potential* (United Nations University/United Nations Institute for Training and Research, International Telecommunication Union, and International Solid Waste Association, 2020).
5. Abdelbasir, S. M., Hassan, S. S. M., Kamel, A. H. & El-Nasr, R. S. Status of electronic waste recycling techniques: a review. *Environ. Sci. Pollut. Res.* **25**, 16533–16547 (2018).
6. Ogunseitan, O. A., Schoenung, J. M., Saphores, J.-D. M. & Shapiro, A. A. The electronics revolution: from e-wonderland to e-wasteland. *Science* **326**, 670–671 (2009).
7. Ogunseitan, O. A. et al. Biobased materials for sustainable printed circuit boards. *Nat. Rev. Mater.* **7**, 749–750 (2022).
8. Yang, C., Li, J., Tan, Q., Liu, L. & Dong, Q. Green process of metal recycling: coprocessing waste printed circuit boards and spent tin stripping solution. *ACS Sustain. Chem. Eng.* **5**, 3524–3534 (2017).
9. Zeng, X., Mathews, J. A. & Li, J. Urban mining of e-waste is becoming more cost-effective than virgin mining. *Environ. Sci. Technol.* **52**, 4835–4841 (2018).
10. Hsu, E., Durning, C. J., West, A. C. & Park, A.-H. A. Enhanced extraction of copper from electronic waste via induced morphological changes using supercritical CO₂. *Resour. Conserv. Recycl.* **168**, 105296 (2021).
11. Shojaeiarani, J., Bajwa, D. S., Rehovsky, C., Bajwa, S. G. & Vahidi, G. Deterioration in the physico-mechanical and thermal properties of biopolymers due to reprocessing. *Polymers* **11**, 58 (2019).
12. Mir, S. & Dhawan, N. A comprehensive review on the recycling of discarded printed circuit boards for resource recovery. *Resour. Conserv. Recycl.* **178**, 106027 (2022).
13. Rocchetti, L., Amato, A. & Beolchini, F. Printed circuit board recycling: a patent review. *J. Clean. Prod.* **178**, 814–832 (2018).
14. Chen, Z. et al. Recycling waste circuit board efficiently and environmentally friendly through small-molecule assisted dissolution. *Sci. Rep.* **9**, 17902 (2019).
15. Khrustalev, D., Tirzhanov, A., Khrustaleva, A., Mustafin, M. & Yedrissov, A. A new approach to designing easily recyclable printed circuit boards. *Sci. Rep.* **12**, 22199 (2022).
16. Ahrens, A. et al. Catalytic disconnection of C–O bonds in epoxy resins and composites. *Nature* **617**, 730–737 (2023).
17. Beeler, B. & Bell, L. Plastic recycling schemes generate high volumes of hazardous waste. *IPEN* <https://ipen.org/news/plastic-recycling-schemes-generate-high-volumes-hazardous-waste> (2021).
18. Kawahara, Y., Hodges, S., Cook, B. S., Zhang, C. & Abowd, G. D. Instant inkjet circuits: lab-based inkjet printing to support rapid prototyping of UbiComp devices. In *Proc. 2013 ACM International Joint Conference on Pervasive and Ubiquitous Computing* 363–372 (Association for Computing Machinery, 2013).
19. Siegel, A. C. et al. Foldable printed circuit boards on paper substrates. *Adv. Funct. Mater.* **20**, 28–35 (2010).
20. Huang, X. et al. Biodegradable materials for multilayer transient printed circuit boards. *Adv. Mater.* **26**, 7371–7377 (2014).
21. Cheng, T. et al. Silver tape: inkjet-printed circuits peeled-and-transferred on versatile substrates. *Proc. ACM Interact. Mob. Wearable Ubiquitous Technol.* **4**, 1–17 (2020).
22. Arroyos, V. et al. A tale of two mice: sustainable electronics design and prototyping. In *Extended Abstracts of the 2022 CHI Conference on Human Factors in Computing Systems* 1–10 (Association for Computing Machinery, 2022).
23. Cheng, T. et al. SwellSense: Creating 2.5D interactions with micro-capsule paper. In *Proc. 2023 CHI Conference on Human Factors in Computing Systems* 1–13 (Association for Computing Machinery, 2023).
24. Kuang, X., Mu, Q., Roach, D. J. & Qi, H. J. Shape-programmable and healable materials and devices using thermo- and photo-responsive vitrimer. *Multifunct. Mater.* **3**, 045001 (2020).
25. Montarnal, D., Capelot, M., Tournilhac, F. & Leibler, L. Silica-like malleable materials from permanent organic networks. *Science* **334**, 965–968 (2011).
26. Zheng, N., Xu, Y., Zhao, Q. & Xie, T. Dynamic covalent polymer networks: a molecular platform for designing functions beyond chemical recycling and self-healing. *Chem. Rev.* **121**, 1716–1745 (2021).
27. Kamble, M. et al. Reversing fatigue in carbon-fiber reinforced vitrimer composites. *Carbon* **187**, 108–114 (2022).
28. Park, S., Kim, S., Han, Y. & Park, J. Apparatus for electronic component disassembly from printed circuit board assembly in e-wastes. *Int. J. Miner. Process.* **144**, 11–15 (2015).
29. Lee, M.-S., Ahn, J.-G. & Ahn, J.-W. Recovery of copper, tin and lead from the spent nitric etching solutions of printed circuit board and regeneration of the etching solution. *Hydrometallurgy* **70**, 23–29 (2003).
30. Zou, Z. et al. Rehealable, fully recyclable, and malleable electronic skin enabled by dynamic covalent thermoset nanocomposite. *Sci. Adv.* **4**, eaaoq0508 (2018).
31. Kehong, F. High performance epoxy copper clad laminate. *Circuit World* **30**, 16–19 (2004).
32. Guerre, M., Taplan, C., Winne, J. M. & Prez, F. E. D. Vitrimers: directing chemical reactivity to control material properties. *Chem. Sci.* **11**, 4855–4870 (2020).
33. Yang, Y., Xu, Y., Ji, Y. & Wei, Y. Functional epoxy vitrimers and composites. *Prog. Mater. Sci.* **120**, 100710 (2021).
34. Liu, T. et al. A self-healable high glass transition temperature bioepoxy material based on vitrimer chemistry. *Macromolecules* **51**, 5577–5585 (2018).
35. Zhang, X. et al. Novel phosphazene-based flame retardant polyimine vitrimers with monomer-recovery and high performances. *Chem. Eng. J.* **440**, 135806 (2022).
36. Daepf, M. I. G. et al. Eclipse: an end-to-end platform for low-cost, hyperlocal environmental sensing in cities. In *2022 21st ACM/IEEE International Conference on Information Processing in Sensor Networks (IPSN)* 28–40 (IEEE, 2022).
37. Hollins, O. Executive summary: an assessment of the greenhouse gas emissions and waste impacts from improving the repairability of microsoft devices (Microsoft Corporation, 2022).
38. Wu, P., Liu, L. & Wu, Z. A transesterification-based epoxy vitrimer synthesis enabled high crack self-healing efficiency to fibrous composites. *Compos. A Appl. Sci. Manuf.* **162**, 107170 (2022).

39. Zhang, D. & Huang, Y. Influence of surface roughness and bondline thickness on the bonding performance of epoxy adhesive joints on mild steel substrates. *Prog. Org. Coat.* **153**, 106135 (2021).
40. DuPont de Nemours, Inc. Recovery of Tetrahydrofuran (THF), Report W-400446 (2000).
41. Hubbard, A. M. et al. Vitrimer transition temperature identification: coupling various thermomechanical methodologies. *ACS Appl. Polym. Mater.* **3**, 1756–1766 (2021).
42. Tian, X., Stranks, S. D. & You, F. Life cycle assessment of recycling strategies for perovskite photovoltaic modules. *Nat. Sustain.* **4**, 821–829 (2021).
43. Weis, V. *Prepreg Shelf Life* (Arlon, 2020).
44. Biswal, A. K., Nandi, A., Wang, H. & Vashisth, A. Ultrasonic welding of fiber reinforced vitrimer composites. *Compos. Sci. Technol.* **242**, 110202 (2023).
45. Lucherelli, M. A., Duval, A. & Avérous, L. Biobased vitrimers: towards sustainable and adaptable performing polymer materials. *Prog. Polym. Sci.* **127**, 101515 (2022).
46. IPC-7711C/7721C Rework, Modification and Repair of Electronic Assemblies (IPC, 2017).
47. IPC TM-650 Test Methods Manual (IPC, 2021).

Acknowledgements

We thank T. Cheng for discussion, Z. Englhardt for help with Bluetooth coding, B. Kuykendall for the use of mechanical testers, C. Li for feedback on the figures, K. Liao and M. Parker for help with flammability testing, and H. Wang for help with composite fabrication. We also thank D. Baker, F. Newman and C. Toskey for help with sputter coating and copper plating. This research was supported by the Microsoft Climate Research Initiative, an Amazon Research Award and the Google Research Scholar Program. Z. Zhang was supported by the University of Washington CEI Fellowship.

Author Contributions

Z.Z., B.H.N., A.V. and V.I. conceptualized, organized and structured the work. Z.Z., A.K.B. and A.N. fabricated GFRV composites. Z.Z. manufactured vitrimer-based PCB and conducted characterizations. Z.Z. designed the hardware system, experiments and evaluations. Z.Z., J.A.S. and B.H.N. designed the repair experiments and evaluations.

Z.Z., A.K.B., J.A.S., B.H.N. and A.V. designed the recycling experiments and evaluations. Z.Z. and A.K.B. conducted material characterizations. K.F. conducted the life-cycle assessment analysis. Z.Z. and V.I. wrote the manuscript. S.P., A.V. and V.I. jointly supervised the work. All authors contributed to the study concept and experimental methods, discussed the results and edited the manuscript.

Competing interests

K.F., J.A.S. and B.H.N. are employees of Microsoft Corporation. S.P. is an employee of Google LLC. Z.Z., A.K.B., A.N., A.V. and V.I. declare no competing interests.

Additional information

Extended data is available for this paper at <https://doi.org/10.1038/s41893-024-01333-7>.

Supplementary information The online version contains supplementary material available at <https://doi.org/10.1038/s41893-024-01333-7>.

Correspondence and requests for materials should be addressed to Aniruddh Vashisth or Vikram Iyer.

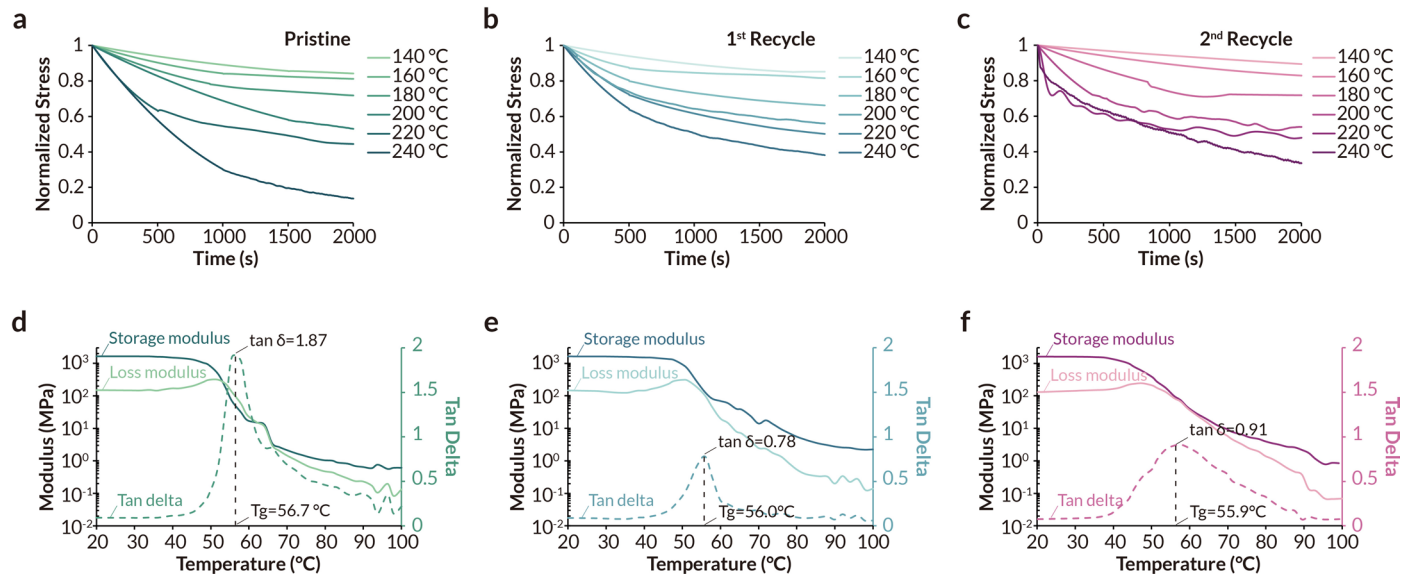
Peer review information *Nature Sustainability* thanks Rasoul Nekouei, Bozhi Tian, Xianlai Zeng and the other, anonymous, reviewer(s) for their contribution to the peer review of this work.

Reprints and permissions information is available at www.nature.com/reprints.

Publisher's note Springer Nature remains neutral with regard to jurisdictional claims in published maps and institutional affiliations.

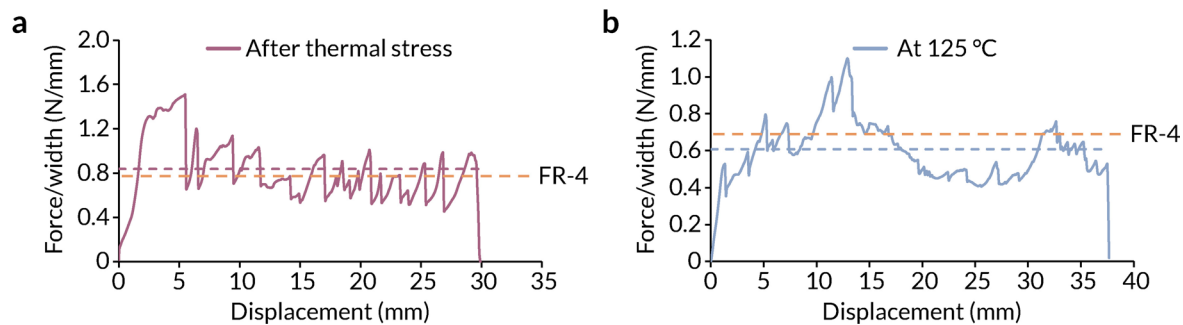
Springer Nature or its licensor (e.g. a society or other partner) holds exclusive rights to this article under a publishing agreement with the author(s) or other rightsholder(s); author self-archiving of the accepted manuscript version of this article is solely governed by the terms of such publishing agreement and applicable law.

© The Author(s), under exclusive licence to Springer Nature Limited 2024

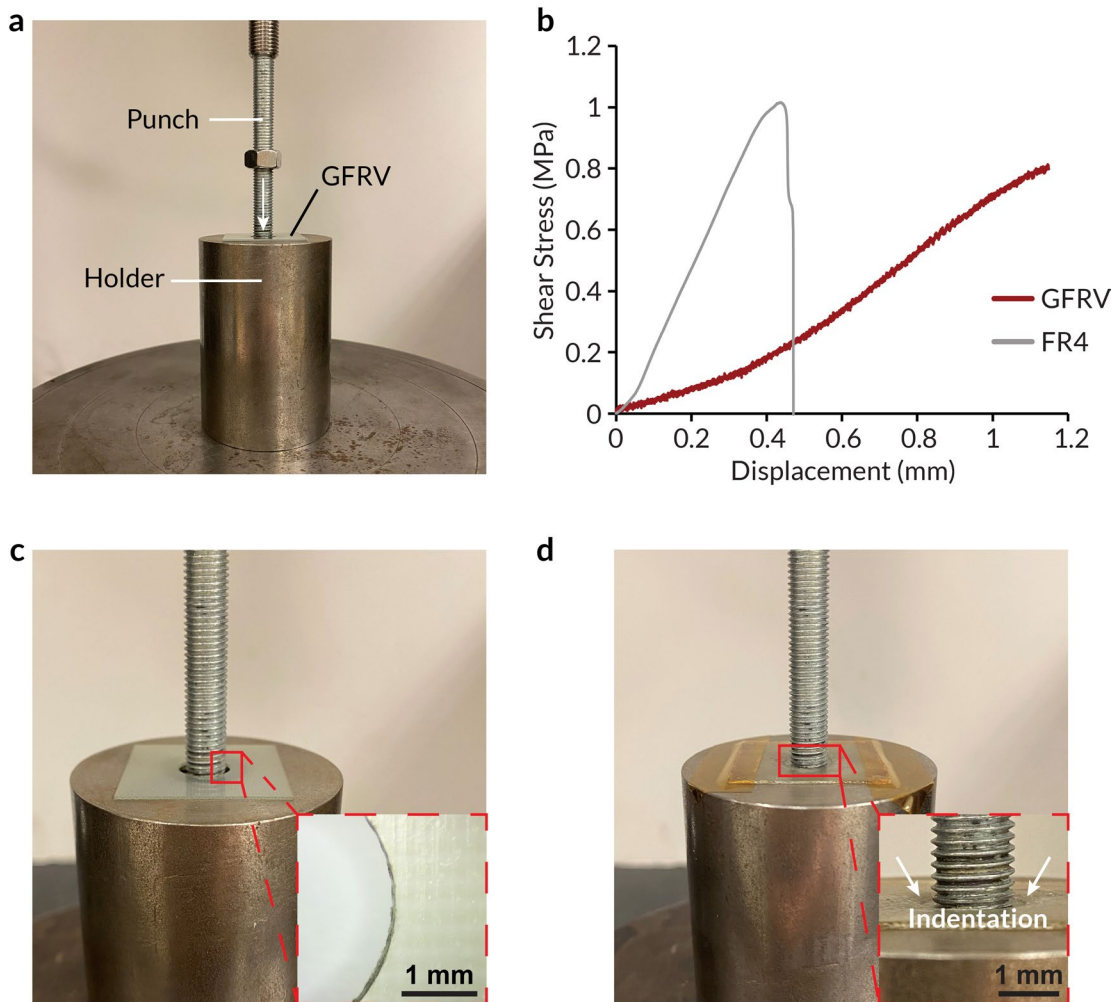


Extended Data Fig. 1 | Dynamic mechanical analysis of pristine and recycled vitrimer. **a, b, c,** Normalized stress relaxation curves of pristine vitrimer (**a**), vitrimer after one recycling cycle (**b**), and vitrimer after two recycling cycles (**c**) at temperatures ranging from 140 °C to 240 °C. In all cases increasing temperature

results in faster stress relaxation. **d, e, f,** Characterized storage modulus, loss modulus, and tan delta of pristine vitrimer (**d**), vitrimer after one recycling cycle (**e**), and vitrimer after two recycling cycles (**f**).

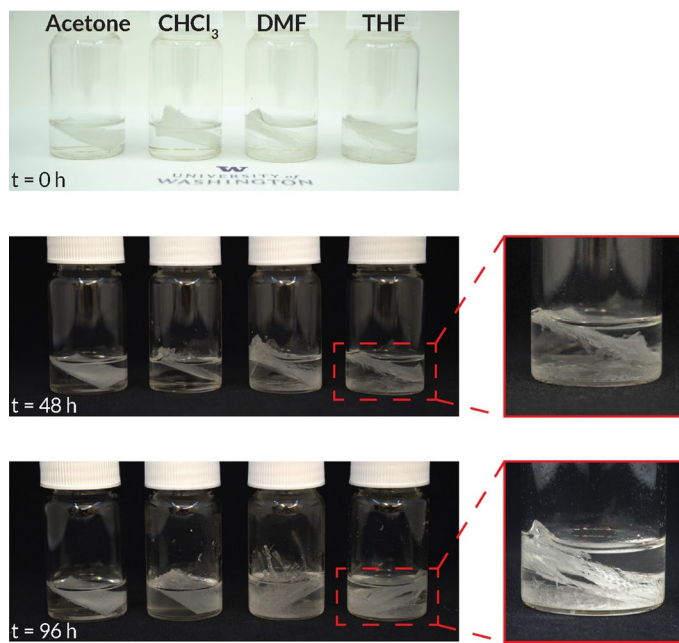


Extended Data Fig. 2 | Peel strength for copper-clad laminates with a layer of partially cured vitrimer. **a, b,** Curves of the peeling force per width of copper-clad versus displacement for laminates with a layer of partially cured vitrimer after thermal stress (**a**), and at 125 °C (**b**) compared to the PCB standard of FR-4.

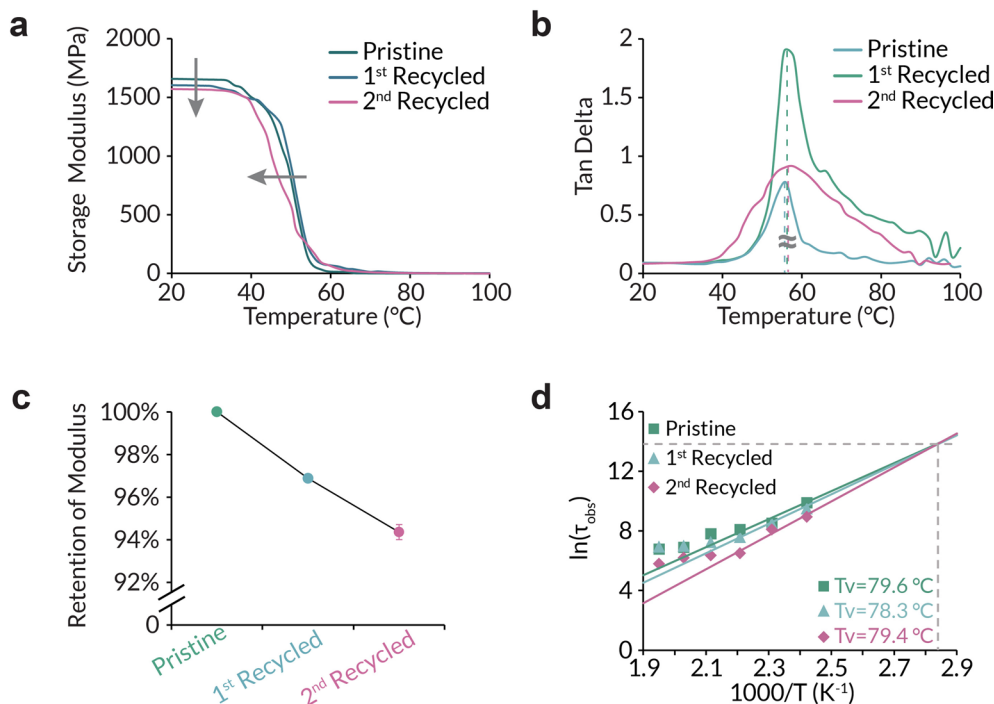
**Extended Data Fig. 3 | Joint strength of repaired via holes in vPCB.**

a, Photograph showing the joint strength testing setup. Specimen is centered on a metal hollow cylinder support with a support span of 16 mm. **b**, Characterized shear stress of repaired via holes in GFRV compared to the repaired holes in FR-4 using super glue.

c, Photograph of FR-4 after shear punch, showing cyanoacrylate glue bond broke. **d**, Photograph of GFRV after shear punch, showing the repaired via hole was deformed into a funnel-shape under the force of punch but remained intact, indicating a stronger interface at the hole boundary.

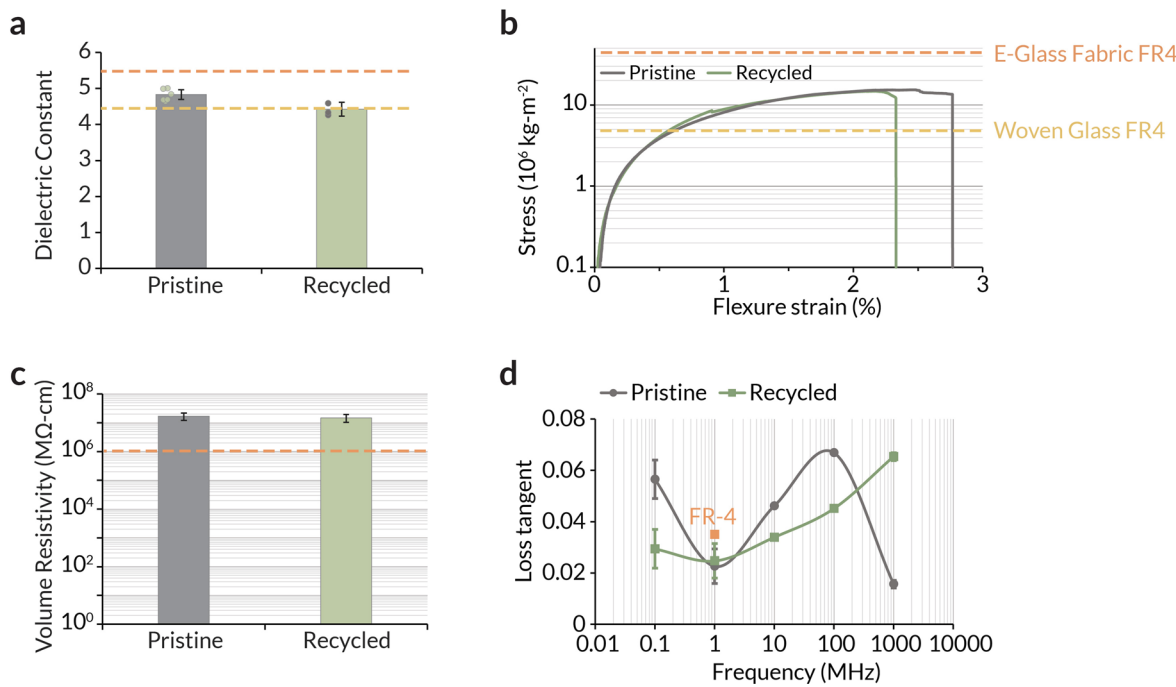


Extended Data Fig. 4 | Solvents test for vPCB recycling. GFRV samples were cut into rectangular shapes and immersed in various solutions (Acetone, CHCl₃, DMF, THF); the top, middle and bottom photos were taken immediately after immersing, after 48 h, and after 96 h, respectively.



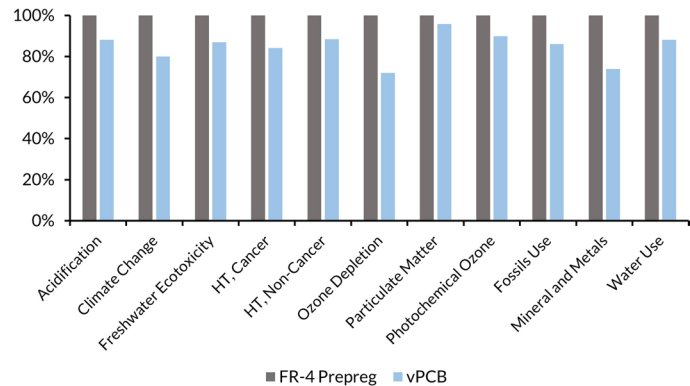
Extended Data Fig. 5 | Characterized storage modulus, tan delta, retention of storage modulus, and vitrimer transition temperature of recycled vitrimer. **a**, Characterized storage modulus temperature sweep results of vitrimer after one and two recycling cycles compared to pristine. The storage modulus shows a slight decrease after recycling. **b**, Tan delta temperature sweep results of vitrimer after one and two recycling cycles compared to pristine, tan delta broadens and the left shift of peaks is negligible after recycling. **c**, Retention of storage

modulus of vitrimer after one and two recycling cycles compared to pristine, data is presented as mean (SD) of vitrimer specimen in 4 parallel experiments ($N=4$). **d**, T_v comparison of pristine vitrimer, vitrimer after one and two recycling cycles, indicating the shift of T_v is negligible after recycling. The Arrhenius plot is derived with a linear fit to the low-temperature region (140 °C to 180 °C), and its intersection with where the stress-relaxation constant is 10^6 indicates the T_v .

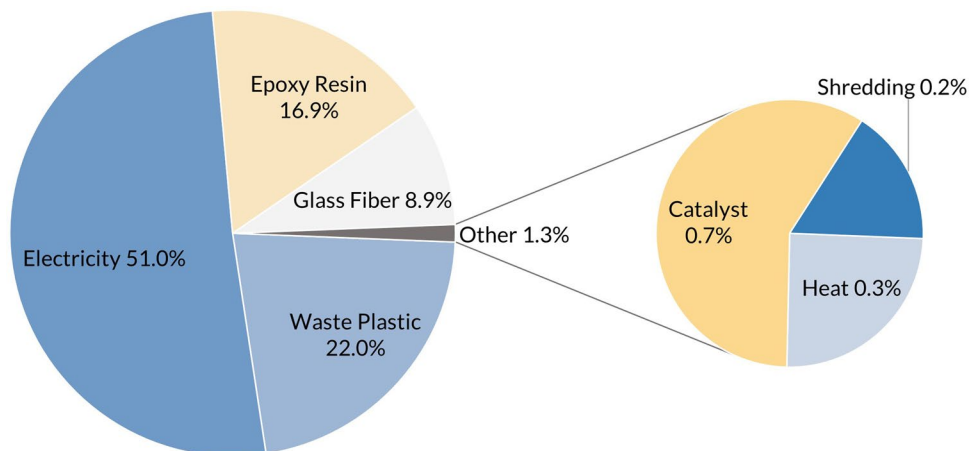


Extended Data Fig. 6 | Characterized electrical and mechanical properties of reformed vPCB. **a, b, c,** Characterized dielectric constant (**a**), flexural strength (**b**), volume resistivity (**c**), and loss tangent (**d**) of reformed GFRV compared to

virgin composite, data is presented as mean (SD) of 3 vPCB specimens in 1 (**a, d**) and 1000 (**c**) measurements ($N = 3, 1000$, and 3 for dielectric constant, resistivity, and loss tangent, respectively).



Extended Data Fig. 7 | Environmental impact of vPCB freight. Comparison of the environmental impact of vPCB freight versus conventional FR-4 prepreg freight across 11 different categories.



Extended Data Fig. 8 | Breakdown of global warming potential for conventional FR-4 PCB. Global warming potential impact breakdown of conventional FR-4 PCB, showing that raw materials account for 48.5% of the total impact.

Reporting Summary

Nature Portfolio wishes to improve the reproducibility of the work that we publish. This form provides structure for consistency and transparency in reporting. For further information on Nature Portfolio policies, see our [Editorial Policies](#) and the [Editorial Policy Checklist](#).

Please do not complete any field with "not applicable" or n/a. Refer to the help text for what text to use if an item is not relevant to your study. For final submission: please carefully check your responses for accuracy; you will not be able to make changes later.

Statistics

For all statistical analyses, confirm that the following items are present in the figure legend, table legend, main text, or Methods section.

- | | |
|-------------------------------------|--|
| n/a | Confirmed |
| <input type="checkbox"/> | <input checked="" type="checkbox"/> The exact sample size (<i>n</i>) for each experimental group/condition, given as a discrete number and unit of measurement |
| <input type="checkbox"/> | <input checked="" type="checkbox"/> A statement on whether measurements were taken from distinct samples or whether the same sample was measured repeatedly |
| <input checked="" type="checkbox"/> | <input checked="" type="checkbox"/> The statistical test(s) used AND whether they are one- or two-sided
<i>Only common tests should be described solely by name; describe more complex techniques in the Methods section.</i> |
| <input checked="" type="checkbox"/> | <input type="checkbox"/> A description of all covariates tested |
| <input checked="" type="checkbox"/> | <input type="checkbox"/> A description of any assumptions or corrections, such as tests of normality and adjustment for multiple comparisons |
| <input type="checkbox"/> | <input checked="" type="checkbox"/> A full description of the statistical parameters including central tendency (e.g. means) or other basic estimates (e.g. regression coefficient) AND variation (e.g. standard deviation) or associated estimates of uncertainty (e.g. confidence intervals) |
| <input checked="" type="checkbox"/> | <input type="checkbox"/> For null hypothesis testing, the test statistic (e.g. <i>F</i> , <i>t</i> , <i>r</i>) with confidence intervals, effect sizes, degrees of freedom and <i>P</i> value noted
<i>Give P values as exact values whenever suitable.</i> |
| <input checked="" type="checkbox"/> | <input type="checkbox"/> For Bayesian analysis, information on the choice of priors and Markov chain Monte Carlo settings |
| <input checked="" type="checkbox"/> | <input type="checkbox"/> For hierarchical and complex designs, identification of the appropriate level for tests and full reporting of outcomes |
| <input checked="" type="checkbox"/> | <input type="checkbox"/> Estimates of effect sizes (e.g. Cohen's <i>d</i> , Pearson's <i>r</i>), indicating how they were calculated |

Our web collection on [statistics for biologists](#) contains articles on many of the points above.

Software and code

Policy information about [availability of computer code](#)

Data collection

The source code is available for download on a public GitHub repository: <https://github.com/iamZhihanZhang/vPCB-IoT-Platform.git>.

Data analysis

Visual Studio Code and Nordic Semiconductors SDK for microcontroller programming, Adafruit BME280 library, GaBi and the Ecoinvent database for LCA and EF method v3.0, Microsoft Office for preparing documents and tables, Adobe Illustrator for preparing figure

For manuscripts utilizing custom algorithms or software that are central to the research but not yet described in published literature, software must be made available to editors and reviewers. We strongly encourage code deposition in a community repository (e.g. GitHub). See the Nature Portfolio [guidelines for submitting code & software](#) for further information.

Data

Policy information about [availability of data](#)

All manuscripts must include a [data availability statement](#). This statement should provide the following information, where applicable:

- Accession codes, unique identifiers, or web links for publicly available datasets
- A description of any restrictions on data availability
- For clinical datasets or third party data, please ensure that the statement adheres to our [policy](#)

All data needed to evaluate the conclusions of the paper are available in the paper or in the Extended Data and Source Data.

Research involving human participants, their data, or biological material

Policy information about studies with [human participants or human data](#). See also policy information about [sex, gender \(identity/presentation\), and sexual orientation](#) and [race, ethnicity and racism](#).

Reporting on sex and gender	n/a
Reporting on race, ethnicity, or other socially relevant groupings	n/a
Population characteristics	n/a
Recruitment	n/a
Ethics oversight	n/a

Note that full information on the approval of the study protocol must also be provided in the manuscript.

Field-specific reporting

Please select the one below that is the best fit for your research. If you are not sure, read the appropriate sections before making your selection.

Life sciences Behavioural & social sciences Ecological, evolutionary & environmental sciences

For a reference copy of the document with all sections, see nature.com/documents/nr-reporting-summary-flat.pdf

Life sciences study design

All studies must disclose on these points even when the disclosure is negative.

Sample size	Sample sizes (N) reported for each experiment in figure legends
Data exclusions	n/a
Replication	All data and information are available
Randomization	n/a
Blinding	n/a

Behavioural & social sciences study design

All studies must disclose on these points even when the disclosure is negative.

Study description	
Research sample	
Sampling strategy	
Data collection	
Timing	
Data exclusions	
Non-participation	
Randomization	

Ecological, evolutionary & environmental sciences study design

All studies must disclose on these points even when the disclosure is negative.

Study description	<input type="text"/>
Research sample	<input type="text"/>
Sampling strategy	<input type="text"/>
Data collection	<input type="text"/>
Timing and spatial scale	<input type="text"/>
Data exclusions	<input type="text"/>
Reproducibility	<input type="text"/>
Randomization	<input type="text"/>
Blinding	<input type="text"/>

Did the study involve field work? Yes No

Field work, collection and transport

Field conditions	<input type="text"/>
Location	<input type="text"/>
Access & import/export	<input type="text"/>
Disturbance	<input type="text"/>

Reporting for specific materials, systems and methods

We require information from authors about some types of materials, experimental systems and methods used in many studies. Here, indicate whether each material, system or method listed is relevant to your study. If you are not sure if a list item applies to your research, read the appropriate section before selecting a response.

Materials & experimental systems		Methods	
n/a	Involved in the study	n/a	Involved in the study
<input checked="" type="checkbox"/>	<input type="checkbox"/> Antibodies	<input checked="" type="checkbox"/>	<input type="checkbox"/> ChIP-seq
<input checked="" type="checkbox"/>	<input type="checkbox"/> Eukaryotic cell lines	<input checked="" type="checkbox"/>	<input type="checkbox"/> Flow cytometry
<input checked="" type="checkbox"/>	<input type="checkbox"/> Palaeontology and archaeology	<input checked="" type="checkbox"/>	<input type="checkbox"/> MRI-based neuroimaging
<input checked="" type="checkbox"/>	<input type="checkbox"/> Animals and other organisms		
<input checked="" type="checkbox"/>	<input type="checkbox"/> Clinical data		
<input checked="" type="checkbox"/>	<input type="checkbox"/> Dual use research of concern		
<input checked="" type="checkbox"/>	<input type="checkbox"/> Plants		

Antibodies

Antibodies used	<input type="text"/>
Validation	<input type="text"/>

Eukaryotic cell lines

Policy information about [cell lines](#) and [Sex and Gender in Research](#)

Cell line source(s)

Authentication

Mycoplasma contamination

Commonly misidentified lines
(See [ICLAC register](#))

Palaeontology and Archaeology

Specimen provenance

Specimen deposition

Dating methods

Tick this box to confirm that the raw and calibrated dates are available in the paper or in Supplementary Information.

Ethics oversight

Note that full information on the approval of the study protocol must also be provided in the manuscript.

Animals and other research organisms

Policy information about [studies involving animals](#); [ARRIVE guidelines](#) recommended for reporting animal research, and [Sex and Gender in Research](#)

Laboratory animals

Wild animals

Reporting on sex

Field-collected samples

Ethics oversight

Note that full information on the approval of the study protocol must also be provided in the manuscript.

Clinical data

Policy information about [clinical studies](#)

All manuscripts should comply with the ICMJE [guidelines for publication of clinical research](#) and a completed [CONSORT checklist](#) must be included with all submissions.

Clinical trial registration

Study protocol

Data collection

Outcomes

Dual use research of concern

Policy information about [dual use research of concern](#)

Hazards

Could the accidental, deliberate or reckless misuse of agents or technologies generated in the work, or the application of information presented in the manuscript, pose a threat to:

No	Yes
<input type="checkbox"/>	<input type="checkbox"/> Public health
<input type="checkbox"/>	<input type="checkbox"/> National security
<input type="checkbox"/>	<input type="checkbox"/> Crops and/or livestock
<input type="checkbox"/>	<input type="checkbox"/> Ecosystems
<input type="checkbox"/>	<input type="checkbox"/> Any other significant area

Experiments of concern

Does the work involve any of these experiments of concern:

No	Yes
<input type="checkbox"/>	<input type="checkbox"/> Demonstrate how to render a vaccine ineffective
<input type="checkbox"/>	<input type="checkbox"/> Confer resistance to therapeutically useful antibiotics or antiviral agents
<input type="checkbox"/>	<input type="checkbox"/> Enhance the virulence of a pathogen or render a nonpathogen virulent
<input type="checkbox"/>	<input type="checkbox"/> Increase transmissibility of a pathogen
<input type="checkbox"/>	<input type="checkbox"/> Alter the host range of a pathogen
<input type="checkbox"/>	<input type="checkbox"/> Enable evasion of diagnostic/detection modalities
<input type="checkbox"/>	<input type="checkbox"/> Enable the weaponization of a biological agent or toxin
<input type="checkbox"/>	<input type="checkbox"/> Any other potentially harmful combination of experiments and agents

Plants

Seed stocks

Novel plant genotypes

Authentication

ChIP-seq

Data deposition

- Confirm that both raw and final processed data have been deposited in a public database such as [GEO](#).
- Confirm that you have deposited or provided access to graph files (e.g. BED files) for the called peaks.

Data access links

May remain private before publication.

Files in database submission

Genome browser session
(e.g. [UCSC](#))

Methodology

Replicates

Sequencing depth

Antibodies

Peak calling parameters

Data quality

Software

Flow Cytometry

Plots

Confirm that:

- The axis labels state the marker and fluorochrome used (e.g. CD4-FITC).
- The axis scales are clearly visible. Include numbers along axes only for bottom left plot of group (a 'group' is an analysis of identical markers).
- All plots are contour plots with outliers or pseudocolor plots.
- A numerical value for number of cells or percentage (with statistics) is provided.

Methodology

Sample preparation

Instrument

Software

Cell population abundance

Gating strategy

Tick this box to confirm that a figure exemplifying the gating strategy is provided in the Supplementary Information.

Magnetic resonance imaging

Experimental design

Design type

Design specifications

Behavioral performance measures

Imaging type(s)

Field strength

Sequence & imaging parameters

Area of acquisition

Diffusion MRI

Used

Not used

Preprocessing

Preprocessing software

Normalization

Normalization template

Noise and artifact removal

Volume censoring

Statistical modeling & inference

Model type and settings

Effect(s) tested

Specify type of analysis: Whole brain ROI-based Both

Statistic type for inference

(See [Eklund et al. 2016](#))

Correction

Models & analysis

n/a Involved in the study

- | | |
|--------------------------|--|
| <input type="checkbox"/> | Functional and/or effective connectivity |
| <input type="checkbox"/> | Graph analysis |
| <input type="checkbox"/> | Multivariate modeling or predictive analysis |

Functional and/or effective connectivity

Graph analysis

Multivariate modeling and predictive analysis

